sciendo

VOLUME 18, N° 4 2024
Journal of Automation, Mobile Robotics and Intelligent Systems

Nonlinear Optimal and Multi-loop Flatness-based Control of Omnidirectional 3-wheel Mobile Robots

Submitted: 25th October 2023; accepted: 24th April 2024

Gerasimos Rigatos, Masoud Abbaszadeh

DOI: 10.14313/JAMRIS/4-2024/29

Abstract:
In this article, the control problem for omnidirectional 3-wheel autonomous mobile robots is solved with the use of (i) a nonlinear optimal control method (ii) a flatness-based control approach which is implemented in successive loops. To apply method (i) that is nonlinear optimal control, the dynamic model of the omnidirectional 3-wheel autonomous mobile robots undergoes approximate linearization at each sampling instant with the use of first-order Taylor series expansion and through the computation of the associated Jacobian matrix. The linearization point is defined by the present value of the system's state vector and by the last sampled value of the control inputs vector. To compute the feedback gains of the optimal controller an algebraic Riccati equation is repetitively solved at each time-step of the control algorithm. The global stability properties of the nonlinear optimal control method are proven through Lyapunov analysis. To implement control method (ii), that is flatness-based control in successive loops, the state-space model of the omnidirectional 3-wheel autonomous mobile robot is separated into chained subsystems, which are connected in cascading loops. Each one of these subsystems can be viewed independently as a differentially flat system and control about it can be performed with inversion of its dynamics as in the case of input-output linearized flat systems. The state variables of the preceding (i-th) subsystem become virtual control inputs for the subsequent (i+1-th) subsystem. In turn, exogenous control inputs are applied to the last subsystem. The whole control method is implemented in successive loops and its global stability properties are also proven through Lyapunov stability analysis. The proposed method achieves trajectory tracking and autonomous navigation for the omnidirectional 3-wheel autonomous mobile robots without the need of diffeomorphisms and complicated state-space model transformations.

Keywords: *omnidirectional 3-wheel autonomous mobile robots, autonomous navigation, differential flatness properties, nonlinear optimal control, flatness-based control in successive loops, global stability*

1. Introduction

The 3-wheel omnidirectional mobile robot is a special type of robotic vehicle that is capable of performing motion in all directions of the horizontal plane without nonholonomic constraints [1-4].

It has three degrees of freedom associated with the cartesian coordinates of its center of gravity in the horizontal plane and with its orientation (heading) angle with respect to the horizontal axis of an inertial coordinates frame [5–7]. Its actuation comes from three DC motors which make the wheels of the mobile robot turn at the specified speed [8–10]. Such mobile robots can be directed precisely along complicated paths and have improved maneuverability [11–14]. To achieve control of such robots and their autonomous navigation along specific trajectories, suitable values for the turn speed of the wheels have to be reached which in turn are associated with specific voltage inputs of its motors [15–17]. Omnidirectional 3-wheel mobile robots are met in several applications associated with patrolling and security tasks, cleaning and disinfecting tasks, with the transfer of products in warehouses and with automated delivery tasks, as well as with several agricultural tasks for instance spraying, weeding or harvesting [18–20]. Omnidirectional 2-wheel mobile robots have nonlinear and multi-variable dynamics and so-far several nonlinear control methods have been proposed about them [21–25]. In certain cases autonomous navigation of 3-wheel omnidirectional mobile robots has been based on state estimation-based control or visual servoing [26–29] . The present article develops and tests two new control methods for the dynamic model of 3-wheel omnidirectional mobile robots. These methods are (i) a novel nonlinear optimal control approach, (ii) a flatness-based control approach which is implemented in successive loops. Both control schemes avoid changes of state variables in the dynamic model of the 3-wheel mobile robot as well as complicated transformations of the state space model of this system.

In the first control method which is proposed by the present article, that is nonlinear optimal control, the dynamic model of the omnidirectional 3-wheel mobile robot undergoes approximate linearization through first-order Taylor series expansion [30–31]. The linearization process takes place at each sampling instance and computes the robot's Jacobian matrices around a temporary operating point which is defined by the present value of its state vector and by the last sampled value of the control inputs vector [32–34].

The modelling error which is due to truncation of higher-order terms in the Taylor series expansion is considered to be a perturbation which is asymptotically compensated by the robustness of the control algorithm. For the approximately linearized model of the omnidirectional robot an H-infinity controller is defined. This controller represents a min-max differential game taking place between (i) the robot's control inputs which try to minimize a cost function that contains a quadratic term of the state vector's tracking error and (ii) the model uncertainty and exogenous perturbation terms which try to maximize this cost function. To compute the controller's feedback gains an algebraic Riccati equation has to be repetitively solved at each time-step of the control algorithm [35–36]. The global stability properties of this control scheme are proven through Lyapunov analysis. At a first stage the H-infinity tracking performance criterion is shown to hold which signifies robustness to model uncertainty and perturbations. Moreover, under moderate conditions, global asymptotic stability is proven [37–38]. The nonlinear optimal control method achieves fast and accurate tracking of reference setpoints by the state variables of the mobile robot under moderate variations of its control inputs. Besides, it achieves minimization of energy dispersion by the actuators of the omnidirectional autonomous vehicle and the improvement of this robot's autonomy and operational capacity.

In the second control method which is proposed by the present article, that is flatness-based control in successive loops, it is shown that the dynamic model of the 3-wheel omnidirectional mobile robot can be decomposed into subsystems which are connected in chained form [36]. In this chained state-space description the state variables of the subsequent (i+1-th) subsystem become virtual control inputs in the preceding (i-th) subsystem. Additionally, the virtual control inputs of the preceding (i-th) subsystem become setpoints for the subsequent (i+1-th) subsystem [39–40]. It is also proven that each one of these subsystems, if viewed independently, is differentially flat. Thus it can be concluded that the individual subsystems are input-output linearizable and a stabilizing flatness-based controller can be designed for each one of them through inversion of their dynamics, as it is commonly done for input-output linearized systems. The real control inputs which are applied to the mobile robot are computed from the last subsystem. Starting from it, the chained state-space description of the mobile robot is traced backwards, that is from the last to the first subsystem, within each sampling period. The global stability properties of this control method are proven through Lyapunov analysis. The flatness-based control method is suboptimal in the sense that it does not target explicitly at the minimization of the variations of the control inputs of the robot, however it also achieves precise tracking of reference trajectories in the 2D plane by the 3-wheel omnidirectional autonomous vehicle.

The structure of the paper is as follows: (i) in Section 2 the dynamic model of the 3-wheel omnidirectional mobile robot is analyzed and the associated state-space model is formulated. In Section 3 a nonlinear optimal controller is designed for the dynamic model of the 3-wheel omnidirectional mobile robot based on the computation of the system's Jacobian matrices. In Section 4 a multi-loop flatness-based controller is designed for the dynamic model of the autonomous robotic vehicle after decomposing its state-space model into subsystens which are connected in chained form and which independently satisfy differential flatness properties. In Section 5 simulation tests are performed to further confirm the fine performance of the two aforementioned control methods. Finally, in Section 6 concluding remarks are stated.

2. Dynamic Model of the 3-wheel Omnidirectional Mobile Robot

2.1. State-space Description of the 3-wheel Omnidirectional Robot

The diagram of the 3-wheel omnidirectional mobile robot is given in Figure 1. The diagram depicts the position (x, y) of the center of gravity of the mobile robot in the horizontal plane and the robot's heading angle θ. Besides, the two coordinate frames which are used in the definition of the robot's kinematic and dynamic model are given, namely the body-fixed reference frame $O_M X_M Y_M$ and the inertial reference frame $O_W X_W Y_W$. The parameters of the dynamic model of the robot are outlined in Table 1 [1],[3]:

The dynamic model of the mobile robot is given by [1],[3]:

$$M(q)\ddot{q} + C(q,\dot{q})\dot{q} + \bar{d} = Bu \tag{1}$$

The disturbances vector $\bar{d} = [d_x, d_y, d_\theta]^T$ comprises friction forces thus taking the form $\bar{d} = [d_1\dot{x}, d_2\dot{y}, d_3\dot{\theta}]^T$. The control inputs vector is $u = [u_1, u_2, u_3]^T$. The inertia matrix M is given by

$$M = \begin{pmatrix} \frac{3}{2}p_0 + m & 0 & 0 \\ 0 & \frac{3}{2}p_0 + m & 0 \\ 0 & 0 & 3L_o^2 + I_v \end{pmatrix} \tag{2}$$

The Coriolis matrix C is given by

$$C = \begin{pmatrix} \frac{3}{2}p_1 & \frac{3}{2}p_m\dot{\theta} & 0 \\ -\frac{3}{2}p_m\dot{\theta} & \frac{3}{2}p_1 & 0 \\ 0 & 0 & 3p_1L_o^2 \end{pmatrix} \tag{3}$$

The control inputs gain matrix B is given by

$$B = p_2 \begin{pmatrix} -\frac{1}{2}cos(\theta) - \frac{\sqrt{3}}{2}sin(\theta) & -\frac{1}{2}cos(\theta) + \frac{\sqrt{3}}{2}sin(\theta) & cos(\theta) \\ -\frac{1}{2}sin(\theta) + \frac{\sqrt{3}}{2}cos(\theta) & -\frac{1}{2}cos(\theta) - \frac{\sqrt{3}}{2}sin(\theta) & sin(\theta) \\ L_o & L_o & L_o \end{pmatrix} \tag{4}$$

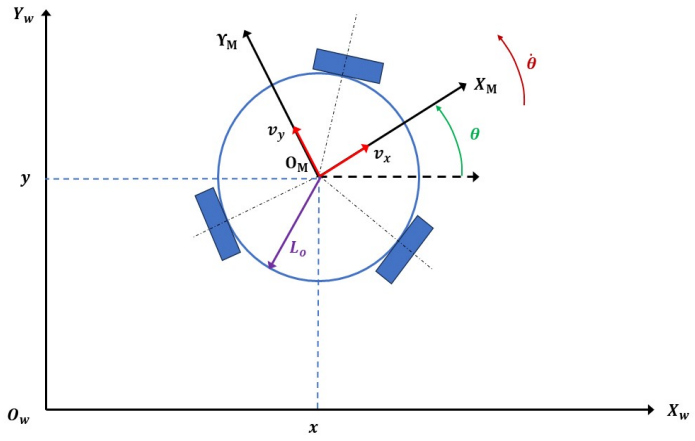

Figure 1. Diagram of the 3-wheel omnidirectional mobile robot and the associated inertial and body-fixed reference frames

Table 1. Dynamic model of 3-wheel omnidirectional robot

Parameter	*Definition*
$q = [x, y, \theta]^T$	robot's position and orientation in inertial frame
$\dot{q} = [\dot{x}, \dot{y}, \dot{\theta}]^T$	robot's linear and angular velocity in inertial frame
$\ddot{q} = [\ddot{x}, \ddot{y}, \ddot{\theta}]^T$	robot's linear and angular acceleration in inertial frame
n	gears reduction ratio between the motors and the wheels
r	radius of the wheels of the omnidirectional robot
m	mass of the omnidirectional robot
I_a	moment of inertia of wheel, gear and motor
k_t, k_b	motors' torque and back EMF constants
I_v	moment of inertia for robot's rotation around the vertical axis
L_o	radius of the robot's cylindrical section
b_a	viscous friction coefficient of wheel, gear and rotor shaft
R_a	resistance of the motors' armature

where coefficients p_0, p_1, p_2 are defined as

$$p_0 = \frac{n^2 I_o}{r^2} \quad p_1 = \frac{\eta^2}{2}\left(b_o + \frac{k_t k_b}{R_a}\right) \quad p_2 = \frac{n k_t}{r R_a} \tag{5}$$

The inverse of the inertia matrix M is given by

$$M^{-1} = \begin{pmatrix} \frac{1}{\frac{3}{2}p_0+m} & 0 & 0 \\ 0 & \frac{1}{\frac{3}{2}p_0+m} & 0 \\ 0 & 0 & \frac{1}{3p_0L_0^2+I_v} \end{pmatrix} \tag{6}$$

Then from Eq. (1) one has the following state-space description:

$$\ddot{q} = -M(q)^{-1}[C(q,\dot{q})\dot{q} + \bar{d}] + M(q)^{-1}Bu \tag{7}$$

which is analytically written in the form

$$\begin{pmatrix} \ddot{x} \\ \ddot{y} \\ \ddot{\theta} \end{pmatrix} = -\begin{pmatrix} \frac{1}{\frac{3}{2}p_0+m} & 0 & 0 \\ 0 & \frac{1}{\frac{3}{2}p_0+m} & 0 \\ 0 & 0 & \frac{1}{3p_0L_0^2+I_v} \end{pmatrix} \left[\begin{pmatrix} \frac{3}{2}p_1 & \frac{3}{2}p_m\dot{\theta} & 0 \\ -\frac{3}{2}p_m\dot{\theta} & \frac{3}{2}p_1 & 0 \\ 0 & 0 & 3p_1L_o^2 \end{pmatrix} \begin{pmatrix} \dot{x} \\ \dot{y} \\ \dot{\theta} \end{pmatrix} + \begin{pmatrix} d_1\dot{x} \\ d_2\dot{y} \\ d_3\dot{\theta} \end{pmatrix} \right]$$

$$+ p_2 \begin{pmatrix} \frac{1}{\frac{3}{2}p_0+m} & 0 & 0 \\ 0 & \frac{1}{\frac{3}{2}p_0+m} & 0 \\ 0 & 0 & \frac{1}{3p_0L_0^2+I_v} \end{pmatrix} \begin{pmatrix} -\frac{1}{2}cos(\theta) - \frac{\sqrt{3}}{2}sin(\theta) \\ -\frac{1}{2}sin(\theta) + \frac{\sqrt{3}}{2}cos(\theta) \\ L_o \end{pmatrix}$$

$$\begin{pmatrix} -\frac{1}{2}cos(\theta) + \frac{\sqrt{3}}{2}sin(\theta) & cos(\theta) \\ -\frac{1}{2}cos(\theta) - \frac{\sqrt{3}}{2}sin(\theta) & sin(\theta) \\ L_o & L_o \end{pmatrix} \begin{pmatrix} u_1 \\ u_2 \\ u_3 \end{pmatrix} \tag{8}$$

After intermediate operations, the state-space description of the 3-wheel omnidirectional robot becomes

$$\begin{pmatrix} \ddot{x} \\ \ddot{y} \\ \ddot{\theta} \end{pmatrix} = \begin{pmatrix} \frac{\frac{3}{2}p_1\dot{x} + \frac{3}{2}p_0\dot{y}\dot{\theta} + d_1\dot{x}}{\frac{3}{2}p_0+m} \\ \frac{-\frac{3}{2}p_0\dot{x}\dot{\theta} + \frac{3}{2}p_1\dot{y} + d_2\dot{y}}{\frac{3}{2}p_0+m} \\ \frac{3p_1L_0^2 + d_3\dot{\theta}}{\frac{3}{2}p_0+m} \end{pmatrix}$$

$$+p_2\begin{pmatrix}\frac{-cos(\theta)-\sqrt{3}sin(\theta)}{2(\frac{3}{2}p_0+m)}\\ \frac{-sin(\theta)+\sqrt{3}cos(\theta)}{2(\frac{3}{2}p_0+m)}\\ \frac{L_o}{3p_0L_o^2+m)}\end{pmatrix}u_1$$

$$+p_2\begin{pmatrix}\frac{-cos(\theta)+\sqrt{3}sin(\theta)}{2(\frac{3}{2}p_0+m)}\\ \frac{-cos(\theta)-\sqrt{3}sin(\theta)}{2(\frac{3}{2}p_0+m)}\\ \frac{L_o}{3p_0L_o^2+m)}\end{pmatrix}u_2$$

$$+p_2\begin{pmatrix}\frac{cos(\theta)}{2(\frac{3}{2}p_0+m)}\\ \frac{sin(\theta)}{2(\frac{3}{2}p_0+m)}\\ \frac{L_o}{3p_0L_o^2+m)}\end{pmatrix}u_3 \quad (9)$$

The state vector of the 3-wheel omnidirectional robot is defined next as

$$x=[x_1,x_2,x_3,x_4,x_5,x_6]^T \Rightarrow x=[x,y,\theta,\dot{x},\dot{y},\dot{\theta}]^T \quad (10)$$

and using this notation, the dynamic model of the mobile robot is written as

$$\begin{pmatrix}\dot{x}_1\\ \dot{x}_2\\ \dot{x}_3\\ \dot{x}_4\\ \dot{x}_5\\ \dot{x}_6\end{pmatrix}=\begin{pmatrix}x_4\\ x_5\\ x_6\\ \frac{\frac{3}{2}p_1x_4+\frac{3}{2}p_0x_5x_6+d_1x_4}{\frac{3}{2}p_0+m}\\ \frac{-\frac{3}{2}p_0x_4x_6+\frac{3}{2}p_1x_5+d_2x_5}{\frac{3}{2}p_0+m}\\ \frac{3p_1L_0^2+d_3x_6}{\frac{3}{2}p_0+m}\end{pmatrix}$$

$$+p_2\begin{pmatrix}0\\ 0\\ 0\\ \frac{-cos(x_3)-\sqrt{3}sin(x_3)}{2(\frac{3}{2}p_0+m)}\\ \frac{-sin(x_3)+\sqrt{3}cos(x_3)}{2(\frac{3}{2}p_0+m)}\\ \frac{L_o}{3p_0L_o^2+m)}\end{pmatrix}u_1$$

$$+p_2\begin{pmatrix}0\\ 0\\ 0\\ \frac{-cos(x_3)+\sqrt{3}sin(x_3)}{2(\frac{3}{2}p_0+m)}\\ \frac{-cos(x_3)-\sqrt{3}sin(x_3)}{2(\frac{3}{2}p_0+m)}\\ \frac{L_o}{3p_0L_o^2+m)}\end{pmatrix}u_2$$

$$+p_2\begin{pmatrix}0\\ 0\\ 0\\ \frac{cos(x_3)}{2(\frac{3}{2}p_0+m)}\\ \frac{sin(x_3)}{2(\frac{3}{2}p_0+m)}\\ \frac{L_o}{3p_0L_o^2+m)}\end{pmatrix}u_3 \quad (11)$$

The dynamic model of the omnidirectional 3-wheel mobile robot can be also written in the nonlinear affine-in-the-input state-space form

$$\dot{x}=f(x)+g_1(x)u_1+g_2(x)u_2+g_3(x)u_3 \quad (12)$$

where $x\in R^{6\times1}$, $f(x)\in R^{6\times1}$, $g_i(x)\in R^{6\times1}$ and $u_i\in R$ for $i=1,2,3$. About vectors $f(x)$ and $g_i(x)$ $i=1,2,3$ one has that

$$f(x)=\begin{pmatrix}x_4\\ x_5\\ x_6\\ \frac{\frac{3}{2}p_1x_4+\frac{3}{2}p_0x_5x_6+d_1x_4}{\frac{3}{2}p_0+m}\\ \frac{-\frac{3}{2}p_0x_4x_6+\frac{3}{2}p_1x_5+d_2x_5}{\frac{3}{2}p_0+m}\\ \frac{3p_1L_0^2+d_3x_6}{\frac{3}{2}p_0+m}\end{pmatrix}$$

$$g_1(x)=p_2\begin{pmatrix}0\\ 0\\ 0\\ \frac{-cos(x_3)-\sqrt{3}sin(x_3)}{2(\frac{3}{2}p_0+m)}\\ \frac{-sin(x_3)+\sqrt{3}cos(x_3)}{2(\frac{3}{2}p_0+m)}\\ \frac{L_o}{3p_0L_o^2+m)}\end{pmatrix}$$

$$g_2(x)=p_2\begin{pmatrix}0\\ 0\\ 0\\ \frac{-cos(x_3)+\sqrt{3}sin(x_3)}{2(\frac{3}{2}p_0+m)}\\ \frac{-cos(x_3)-\sqrt{3}sin(x_3)}{2(\frac{3}{2}p_0+m)}\\ \frac{L_o}{3p_0L_o^2+m)}\end{pmatrix}$$

$$g_3(x)=p_2\begin{pmatrix}0\\ 0\\ 0\\ \frac{cos(x_3)}{2(\frac{3}{2}p_0+m)}\\ \frac{sin(x_3)}{2(\frac{3}{2}p_0+m)}\\ \frac{L_o}{3p_0L_o^2+m)}\end{pmatrix} \quad (13)$$

Additionally, using that the control inputs gain matrix of the mobile robot is $g(x)=[g_1(x),g_2(x),g_3(x)]$ one has

$$\dot{x}=f(x)+g(x)u \quad (14)$$

2.2. Differential Flatness of the 3-wheel Omnidirectional Mobile Robot

The dynamic model of the 3-wheel omnidirectional mobile robot that was given in Eq. (11) is differentially flat, with flat outputs vector $Y = [x_1, x_2, x_3]^T$ or $Y = [x, y, \theta]^T$. Indeed from the first three rows of the state-space description of Eq. (11) one obtains that

$$x_4 = \dot{x}_1 \quad x_5 = \dot{x}_2 \quad x_6 = \dot{x}_3 \tag{15}$$

which signifies that state variables x_4, x_5, x_6 are differential functions of the flat outputs vector Y. Moreover, from the last three rows of the state-space model of the system one has that

$$\begin{pmatrix} u_1 \\ u_2 \\ u_3 \end{pmatrix} = \begin{pmatrix} \frac{-cos(x_3)-\sqrt{3}sin(x_3)}{2(\frac{3}{2}p_0+m)} \\ \frac{-sin(x_3)+\sqrt{3}cos(x_3)}{2(\frac{3}{2}p_0+m)} \\ \frac{L_o}{3p_0L_o^2+m)} \end{pmatrix}$$

$$\begin{pmatrix} \frac{-cos(x_3)+\sqrt{3}sin(x_3)}{2(\frac{3}{2}p_0+m)} & \frac{cos(x_3)}{2(\frac{3}{2}p_0+m)} \\ \frac{-cos(x_3)-\sqrt{3}sin(x_3)}{2(\frac{3}{2}p_0+m)} & \frac{sin(x_3)}{2(\frac{3}{2}p_0+m)} \\ \frac{L_o}{3p_0L_o^2+m)} & \frac{L_o}{3p_0L_o^2+m)} \end{pmatrix}^{-1}$$

$$\left[\begin{pmatrix} \dot{x}_4 \\ \dot{x}_5 \\ \dot{x}_6 \end{pmatrix} - \begin{pmatrix} \frac{\frac{3}{2}p_1x_4+\frac{3}{2}p_0x_5x_6+d_1x_4}{\frac{3}{2}p_0+m} \\ \frac{-\frac{3}{2}p_0x_4x_6+\frac{3}{2}p_1x_5+d_2x_5}{\frac{3}{2}p_0+m} \\ \frac{3p_1L_0^2+d_3x_6}{\frac{3}{2}p_0+m} \end{pmatrix} \right] \tag{16}$$

where all terms that appear in the right part of Eq. (16) are differential functions of the flat outputs vector, consequently the control inputs u_1, u_2, u_3 are also differential functions of the flat outputs vector Y. Therefore, the entire dynamic model of the 3-wheel omnidirectional mobile robot is a differentially flat system.

The differential flatness property is an implicit proof of the system's controllability, as well as of its input-output linearizability. It also allows for solving the setpoints definition problem.

3. Design of a Nonlinear Optimal Controller

3.1. Approximate Linearization of the Dynamics of the 3-wheel Omnidirectional Robot

The dynamic model of the 3-wheel omnidirectional mobile robot undergoes approximate linearization around the temporary operating point (x^*, u^*) which is defined at each sampling instant by the present value of the system's state vector x^* and by the last sampled value of the control inputs vector u^*. The linearization process is based on first-order Taylor series expansion and on the computation of the associated Jacobian matrices.

The modelling error which is due to the truncation of higher-order terms from the Taylor series is considered to be a perturbation which is asymptotically compensated by the robustness of the control algorithm. The initial nonlinear state-space model of the system of Eq. (14) in the form $\dot{x} = f(x) + g(x)u$, is turned into the equivalent linearized state-space form

$$\dot{x} = Ax + Bu + \tilde{d} \tag{17}$$

where $\tilde{d}$ is the cumulative disturbances vector which may comprise (i) modelling error due to the truncation of higher-order terms from the Taylor series, (ii) exogenous perturbations, (iii) sensor measurement noise of any distribution. The Jacobian matrices of the system are given by:

$$\begin{aligned} A &= \nabla_x[f(x) + g(x)u] \mid_{(x^*,u^*)} \Rightarrow \\ A &= \nabla_x f(x) \mid_{(x^*,u^*)} + \nabla_x g_1(x)u_1 \mid_{(x^*,u^*)} \\ &\quad + \nabla_x g_2(x)u_2 \mid_{(x^*,u^*)} + \nabla_x g_3(x)u_3 \mid_{(x^*,u^*)} \end{aligned} \tag{18}$$

$$B = \nabla_u[f(x) + g(x)u] \mid_{(x^*,u^*)} \Rightarrow B = g(x) \mid_{(x^*,u^*)} \tag{19}$$

The linearization approach which has been followed for implementing the nonlinear optimal control scheme results into a quite accurate model of the system's dynamics. Consider for instance the following affine-in-the-input state-space model

$$\begin{aligned} \dot{x} &= f(x) + g(x)u \Rightarrow \\ \dot{x} &= [f(x^*) + \nabla_x f(x) \mid_{x^*} (x - x^*)] + [g(x^*) \\ &\quad + \nabla_x g(x) \mid_{x^*} (x - x^*)]u^* + g(x^*)u^* \\ &\quad + g(x^*)(u - u^*) + \tilde{d}_1 \Rightarrow \\ \dot{x} &= [\nabla_x f(x) \mid_{x^*} + \nabla_x g(x) \mid_{x^*} u^*]x + g(x^*)u \\ &\quad - [\nabla_x f(x) \mid_{x^*} + \nabla_x g(x) \mid_{x^*} u^*]x^* + f(x^*) \\ &\quad + g(x^*)u^* + \tilde{d}_1 \end{aligned} \tag{20}$$

where $\tilde{d}_1$ is the modelling error due to truncation of higher order terms in the Taylor series expansion of $f(x)$ and $g(x)$. Next, by defining $A = [\nabla_x f(x) \mid_{x^*} + \nabla_x g(x) \mid_{x^*} u^*]$, $B = g(x^*)$ one obtains

$$\dot{x} = Ax + Bu - Ax^* + f(x^*) + g(x^*)u^* + \tilde{d}_1 \tag{21}$$

Moreover by denoting $\tilde{d} = -Ax^* + f(x^*) + g(x^*)u^* + \tilde{d}_1$ about the cumulative modelling error term in the Taylor series expansion procedure one has

$$\dot{x} = Ax + Bu + \tilde{d} \tag{22}$$

which is the approximately linearized model of the dynamics of the system of Eq. (14). The term $f(x^*) + g(x^*)u^*$ is the derivative of the state vector at (x^*, u^*) which is almost annihilated by $-Ax^*$.

The Jacobian matrices of the linearized mobile robot are computed as follows:

Computation of the Jacobian matrix $\nabla_x f(x)\mid_{(x^*,u^*)}$:

$$\nabla_x f(x)\mid_{(x^*,u^*)}=\begin{pmatrix} 0&0&0&1&0&0\\ 0&0&0&0&1&0\\ 0&0&0&0&0&1\\ 0&0&0&\frac{\frac{3}{2}p_1+d_1}{\frac{3}{2}p_0+m}&\frac{\frac{3}{2}p_0x_6}{\frac{3}{2}p_0+m}&\frac{\frac{3}{2}p_0x_5}{\frac{3}{2}p_0+m}\\ 0&0&0&\frac{-\frac{3}{2}p_0x_6}{\frac{3}{2}p_0+m}&\frac{\frac{3}{2}p_1+d_2}{\frac{3}{2}p_0+m}&\frac{-\frac{3}{2}p_0x_4}{\frac{3}{2}p_0+m}\\ 0&0&0&0&0&\frac{d_3}{3p_0L_0^2+I_v} \end{pmatrix} \quad (23)$$

Computation of the Jacobian matrix $\nabla_x g_1(x)\mid_{(x^*,u^*)}$:

$$\nabla_x g_1(x)\mid_{(x^*,u^*)}=\begin{pmatrix} 0&0&0&0&0&0\\ 0&0&0&0&0&0\\ 0&0&0&0&0&0\\ 0&0&0&\frac{sin(x_3)+\sqrt{3}cos(x_3)}{2(\frac{3}{2}p_0+m)}&0&0\\ 0&0&0&\frac{-cos(x_3)-\sqrt{3}sin(x_3)}{2(\frac{3}{2}p_0+m)}&0&0\\ 0&0&0&0&0&0 \end{pmatrix} \quad (24)$$

Computation of the Jacobian matrix $\nabla_x g_2(x)\mid_{(x^*,u^*)}$:

$$\nabla_x g_2(x)\mid_{(x^*,u^*)}=\begin{pmatrix} 0&0&0&0&0&0\\ 0&0&0&0&0&0\\ 0&0&0&0&0&0\\ 0&0&0&\frac{sin(x_3)+\sqrt{3}cos(x_3)}{2(\frac{3}{2}p_0+m)}&0&0\\ 0&0&0&\frac{sin(x_3)-\sqrt{3}cos(x_3)}{2(\frac{3}{2}p_0+m)}&0&0\\ 0&0&0&0&0&0 \end{pmatrix} \quad (25)$$

Computation of the Jacobian matrix $\nabla_x g_3(x)\mid_{(x^*,u^*)}$:

$$\nabla_x g_3(x)\mid_{(x^*,u^*)}=\begin{pmatrix} 0&0&0&0&0&0\\ 0&0&0&0&0&0\\ 0&0&0&0&0&0\\ 0&0&0&\frac{-sin(x_3)}{(\frac{3}{2}p_0+m)}&0&0\\ 0&0&0&\frac{cos(x_3)}{(\frac{3}{2}p_0+m)}&0&0\\ 0&0&0&0&0&0 \end{pmatrix} \quad (26)$$

3.2. Stabilizing Feedback Control

After linearization around its current operating point (x^*, u^*), the dynamic model of the 3-wheel omnidirectional mobile robot is written as [30]

$$\dot{x} = Ax + Bu + d_1 \quad (27)$$

Parameter d_1 stands for the linearization error in the 3-wheel omnidirectional mobile robot's model appearing previously in Eq. (27). The reference setpoints for the 3-wheel omnidirectional mobile robot's state vector are denoted by $\boldsymbol{x_d} = [x_1^d, \cdots, x_6^d]$. Tracking of this trajectory is achieved after applying the control input u^*.

At every time instant the control input u^* is assumed to differ from the control input u appearing in Eq. (27) by an amount equal to Δu, that is $u^* = u + \Delta u$

$$\dot{x}_d = Ax_d + Bu^* + d_2 \quad (28)$$

The dynamics of the controlled system described in Eq. (27) can be also written as

$$\dot{x} = Ax + Bu + Bu^* - Bu^* + d_1 \quad (29)$$

and by denoting $d_3 = -Bu^* + d_1$ as an aggregate disturbance term one obtains

$$\dot{x} = Ax + Bu + Bu^* + d_3 \quad (30)$$

By subtracting Eq. (28) from Eq. (30) one has

$$\dot{x} - \dot{x}_d = A(x - x_d) + Bu + d_3 - d_2 \quad (31)$$

By denoting the tracking error as $e = x - x_d$ and the aggregate disturbance term as $L\tilde{d} = d_3 - d_2$, the tracking error dynamics becomes

$$\dot{e} = Ae + Bu + L\tilde{d} \quad (32)$$

where L is the disturbance input gain matrix. For the approximately linearized model of the system a stabilizing feedback controller is developed. The controller has the form

$$u(t) = -Ke(t) \quad (33)$$

with $K = \frac{1}{r}B^TP$ where P is a positive definite symmetric matrix which is obtained from the solution of the Riccati equation [30]

$$A^TP + PA + Q - P(\frac{2}{r}BB^T - \frac{1}{\rho^2}LL^T)P = 0 \quad (34)$$

The previously analyzed concept about the nonlinear optimal control loop for the three-wheel omnidirectional mobile robot is given in Figure 2.
where Q is a positive semi-definite symmetric matrix. Whereas the Linear Quadratic Regulator (LQR) is the solution of the quadratic optimal control problem using Bellman's optimality principle, H-infinity control is the solution of the optimal control problem under model uncertainty and external perturbations. The cost function that is subject to minimization in the case of LQR comprises a quadratic term of the state vector's tracking error, as well as a quadratic term of the variations of the control inputs. In the case of H-infinity control the cost function is extended with the inclusion of a quadratic term of the cumulative disturbance and model uncertainty inputs that affect the model of the controlled system.

In the case of the 3-wheel omnidirectional mobile robot, the vehicle's dynamic model is nonlinear and is also affected by uncertainty and external perturbations. By applying approximate linearization to the 3-wheel omnidirectional mobile robot's dynamics one obtains a linear state-space description which is subject to modelling imprecision and exogenous disturbances. Therefore, one can arrive at a solution of the related optimal control problem only by applying the H-infinity control approach.

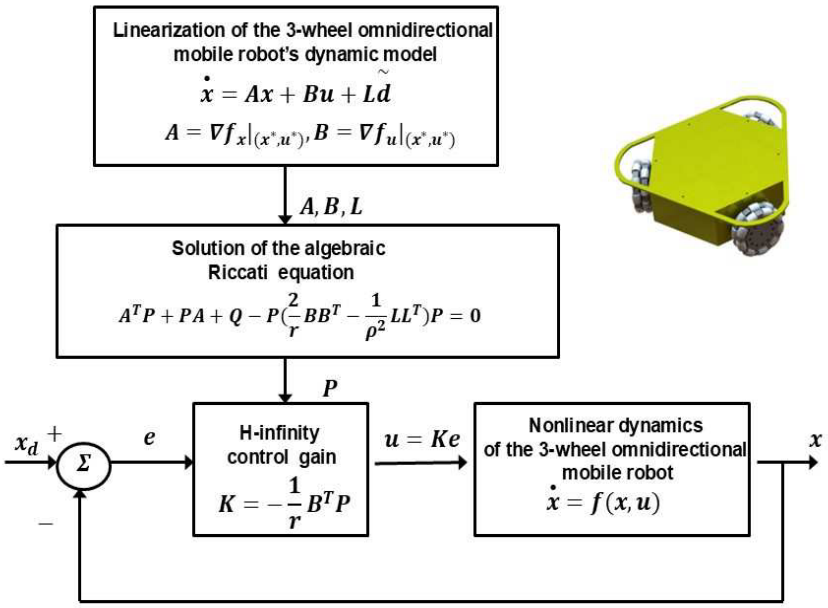

Figure 2. Diagram of the nonlinear optimal control scheme for the omnidirectional three-wheel mobile robot [Source: Authors' own work]

It is also noted that the solution of the H-infinity feedback control problem for the 3-wheel omnidirectional mobile robot and the computation of the worst case disturbance that this controller can sustain, comes from superposition of Bellman's optimality principle when considering that the robot is affected by two separate inputs (i) the control input u (ii) the cumulative disturbance input $\tilde{d}(t)$. Solving the optimal control problem for u that is for the minimum variation (optimal) control input that achieves elimination of the state vector's tracking error gives $u = -\frac{1}{r}B^TPe$. Equivalently, solving the optimal control problem for $\tilde{d}$, that is for the worst case disturbance that the control loop can sustain gives $\tilde{d} = \frac{1}{\rho^2}L^TPe$.

3.3. Lyapunov Stability Analysis

Through Lyapunov stability analysis it will be shown that the proposed nonlinear control scheme assures H_∞ tracking performance for the 3-wheel omnidirectional mobile robot, and that in case of bounded disturbance terms asymptotic convergence to the reference setpoints is achieved. The tracking error dynamics for the 3-wheel omnidirectional mobile robot is written in the form

$$\dot{e} = Ae + Bu + L\tilde{d} \tag{35}$$

where in the 3-wheel omnidirectional mobile robot's case $L = I \in R^{6\times 6}$ with I being the identity matrix. Variable $\tilde{d}$ denotes model uncertainties and external disturbances of the 3-wheel omnidirectional mobile robot's model. The following Lyapunov equation is considered

$$V = \frac{1}{2}e^TPe \tag{36}$$

where $e = x - x_d$ is the tracking error. By differentiating with respect to time one obtains

$$\dot{V} = \frac{1}{2}\dot{e}^TPe + \frac{1}{2}e^TP\dot{e} \Rightarrow$$

$$\dot{V} = \frac{1}{2}[Ae + Bu + L\tilde{d}]^TPe + \frac{1}{2}e^TP[Ae + Bu + L\tilde{d}] \Rightarrow$$

$$\dot{V} = \frac{1}{2}[e^TA^T + u^TB^T + \tilde{d}^TL^T]Pe + \frac{1}{2}e^TP[Ae + Bu + L\tilde{d}] \Rightarrow$$

$$\dot{V} = \frac{1}{2}e^TA^TPe + \frac{1}{2}u^TB^TPe + \frac{1}{2}\tilde{d}^TL^TPe + \frac{1}{2}e^TPAe + \frac{1}{2}e^TPBu + \frac{1}{2}e^TPL\tilde{d} \tag{37}$$

The previous equation is rewritten as

$$\dot{V} = \frac{1}{2}e^T(A^TP + PA)e + (\frac{1}{2}u^TB^TPe + \frac{1}{2}e^TPBu) + (\frac{1}{2}\tilde{d}^TL^TPe + \frac{1}{2}e^TPL\tilde{d}) \tag{38}$$

Assumption: For given positive definite matrix Q and coefficients r and ρ there exists a positive definite matrix P, which is the solution of the following matrix equation

$$A^TP + PA = -Q + P(\frac{2}{r}BB^T - \frac{1}{\rho^2}LL^T)P \tag{39}$$

Moreover, the following feedback control law is applied to the system

$$u = -\frac{1}{r}B^TPe \tag{40}$$

By substituting Eq. (39) and Eq. (40) into Eq. (38) and by performing intermediate operations one obtains

$$\dot{V} = \frac{1}{2}e^T[-Q + P(\frac{2}{r}BB^T - \frac{1}{2\rho^2}LL^T)P]e + e^TPB(-\frac{1}{r}B^TPe) + e^TPL\tilde{d} \Rightarrow$$
$$\dot{V} = -\frac{1}{2}e^TQe + (\frac{1}{r}e^TPBB^TPe - \frac{1}{2\rho^2}e^TPLL^TPe) - \frac{1}{r}e^TPBB^TPe) + e^TPL\tilde{d} \Rightarrow$$
$$\dot{V} = -\frac{1}{2}e^TQe - \frac{1}{2\rho^2}e^TPLL^TPe + e^TPL\tilde{d} \Rightarrow$$
$$\dot{V} = -\frac{1}{2}e^TQe - \frac{1}{2\rho^2}e^TPLL^TPe + \frac{1}{2}e^TPL\tilde{d} + \frac{1}{2}\tilde{d}^TL^TPe \quad (41)$$

Lemma: The following inequality holds

$$\frac{1}{2}e^TPL\tilde{d} + \frac{1}{2}\tilde{d}L^TPe - \frac{1}{2\rho^2}e^TPLL^TPe \leq \frac{1}{2}\rho^2\tilde{d}^T\tilde{d} \quad (42)$$

Proof: The binomial $(\rho\alpha - \frac{1}{\rho}b)^2$ is considered. Expanding the left part of the above inequality one gets

$$\rho^2a^2 + \frac{1}{\rho^2}b^2 - 2ab \geq 0 \Rightarrow \frac{1}{2}\rho^2a^2 + \frac{1}{2\rho^2}b^2 - ab \geq 0 \Rightarrow$$
$$ab - \frac{1}{2\rho^2}b^2 \leq \frac{1}{2}\rho^2a^2 \Rightarrow \frac{1}{2}ab + \frac{1}{2}ab - \frac{1}{2\rho^2}b^2 \leq \frac{1}{2}\rho^2a^2 \quad (43)$$

The following substitutions are carried out: $a = \tilde{d}$ and $b = e^TPL$ and the previous relation becomes

$$\frac{1}{2}\tilde{d}^TL^TPe + \frac{1}{2}e^TPL\tilde{d} - \frac{1}{2\rho^2}e^TPLL^TPe \leq \frac{1}{2}\rho^2\tilde{d}^T\tilde{d} \quad (44)$$

Eq. (44) is substituted in the last row of Eq. (41) and the inequality is enforced, thus giving

$$\dot{V} \leq -\frac{1}{2}e^TQe + \frac{1}{2}\rho^2\tilde{d}^T\tilde{d} \quad (45)$$

Eq. (45) shows that the H_∞ tracking performance criterion is satisfied. The integration of $\dot{V}$ from 0 to T gives

$$\int_0^T \dot{V}(t)dt \leq -\frac{1}{2}\int_0^T ||e||_Q^2 dt + \frac{1}{2}\rho^2\int_0^T ||\tilde{d}||^2 dt \Rightarrow$$
$$2V(T) + \int_0^T ||e||_Q^2 dt \leq 2V(0) + \rho^2\int_0^T ||\tilde{d}||^2 dt \quad (46)$$

Moreover, if there exists a positive constant $M_d > 0$ such that $\int_0^\infty ||\tilde{d}||^2 dt \leq M_d$ then one gets

$$\int_0^\infty ||e||_Q^2 dt \leq 2V(0) + \rho^2 M_d \quad (47)$$

Thus, the integral $\int_0^\infty ||e||_Q^2 dt$ is bounded. Moreover, $V(T)$ is bounded and from the definition of the Lyapunov function V in Eq. (36) it becomes clear that $e(t)$ will be also bounded since $e(t) \in \Omega_e = \{e | e^TPe \leq 2V(0) + \rho^2 M_d\}$. According to the above and with the use of Barbalat's Lemma one obtains $lim_{t\to\infty} e(t) = 0$.

By following the stages of the stability proof one arrives at Eq. (45) which shows that the H-infinity tracking performance criterion holds. By selecting the attenuation coefficient ρ to be sufficiently small and in particular to satisfy $\rho^2 < ||e||_Q^2 / ||\tilde{d}||^2$ one has that the first derivative of the Lyapunov function is upper bounded by 0. This condition holds at each sampling instance and consequently global stability for the control loop can be concluded.

The nonlinear optimal control approach exhibits advantages against other control schemes one could have considered for the dynamics of the 3-wheel omnidirectional mobile robot. For instance: (1) Compared to feedback linearization with the computed-torque method the article's approach achieves minimization of the variations of the control inputs and elimination of energy dispersion by the actuators of the mobile robot. The article's nonlinear optimal control avoids also inverse transformations which may come against singularity problems (2) compared to the global linearization-based control schemes (such as Lie algebra-based control or flatness-based control with transformation into canonical forms) it does not require complicated changes of state variables (diffeomorphisms) and transformation of the system's state-space description. (3) compared to Nonlinear Model Predictive Control, the proposed nonlinear optimal control method is of proven global stability and the convergence of its iterative search for an optimum does not depend on initialization and controller's parametrization, (4) compared to sliding-mode control and backstepping control the application of the nonlinear optimal control method is not constrained into dynamical systems of a specific state-space form. It is known that unless the controlled system is found in the input-output linearized form the definition of the associated sliding surfaces is an empirical procedure. Besides, unless the controlled system is found in the backstepping integral (triangular) form, the application of backstepping control is not possible (5) compared to PID control the nonlinear optimal control method is of proven global stability and its performance is not dependant on heuristics-based selection of parameters of the controller, (6) compared to multiple-models based optimal control, the nonlinear optimal control method requires the computation of only one linearization point and the solution of only one Riccati equation.

4. Design of a Multi-loop Flatness-based Controller for the 3-wheel Robot

The dynamic model of the 3-wheel omnidirectional mobile robot can be decomposed into two chained subsystems Σ_1 and Σ_2, while it can be also demonstrated that for each one of these subsystems differential flatness properties hold. First, subsystem Σ_1 is defined, which comprises the first three rows of the state-space model of Eq. (11).

The following subvectors and submatrices are defined:

$$x_{1,3}=\begin{pmatrix}x_1\\x_2\\x_3\end{pmatrix}\quad f_{1,3}=\begin{pmatrix}0\\0\\0\end{pmatrix}\quad g_{1,3}=\begin{pmatrix}1&0&0\\0&1&0\\0&0&1\end{pmatrix}$$

$$v_1=\begin{pmatrix}x_4\\x_5\\x_6\end{pmatrix} \tag{48}$$

where v_1 is a virtual control input comprising the state variables of the last three rows of the state-space model of Eq. (11). Next, subsystem Σ_2 is considered and the following subvectors and submatrices are defined

$$x_{4,6}=\begin{pmatrix}x_4\\x_5\\x_6\end{pmatrix}\quad f_{4,6}=\begin{pmatrix}\frac{\frac{3}{2}p_1x_4+\frac{3}{2}p_0x_5x_6+d_1x_4}{\frac{3}{2}p_0+m}\\\frac{-\frac{3}{2}p_0x_4x_6+\frac{3}{2}p_1x_5+d_2x_5}{\frac{3}{2}p_0+m}\\\frac{3p_1L_0^2+d_3x_6}{\frac{3}{2}p_0+m}\end{pmatrix} \tag{49}$$

$$g_{4,6}=\begin{pmatrix}\frac{-cos(x_3)-\sqrt{3}sin(x_3)}{2(\frac{3}{2}p_0+m)}&\frac{-cos(x_3)+\sqrt{3}sin(x_3)}{2(\frac{3}{2}p_0+m)}&\frac{cos(x_3)}{2(\frac{3}{2}p_0+m)}\\\frac{-sin(x_3)+\sqrt{3}cos(x_3)}{2(\frac{3}{2}p_0+m)}&\frac{-cos(x_3)-\sqrt{3}sin(x_3)}{2(\frac{3}{2}p_0+m)}&\frac{sin(x_3)}{2(\frac{3}{2}p_0+m)}\\\frac{L_o}{3p_0L_o^2+m)}&\frac{L_o}{3p_0L_o^2+m)}&\frac{L_o}{3p_0L_o^2+m)}\end{pmatrix}$$

$$u=\begin{pmatrix}u_1\\u_2\\u_3\end{pmatrix} \tag{50}$$

where u is the vector of real control inputs. As a result of the above, the dynamics of the omnidirectional robot can be written in the form of two chained subsystems:

$$\dot{x}_{1,3}=f_{1,3}(x_{1,3})+g_{1,3}(x_{1,3})v_1 \tag{51}$$

$$\dot{x}_{4,6}=f_{4,6}(x_{1,3},x_{4,6})+g_{4,6}(x_{1,3},x_{4,6})u \tag{52}$$

It can be proven that each one of subsystems Σ_1 and Σ_2 is differentially flat. For subsystem Σ_1 the flat output is $Y_1=x_{1,3}$. Solving for the virtual control input v_1 one has

$$v_1=g_{1,3}(x_{1,3})^{-1}[\dot{x}_{1,3}-f_{1,3}(x_{1,3})] \tag{53}$$

which signifies that $v_1=x_{4,6}$ is a differential function of $Y_1=x_{1,3}$ (indeed it holds $v_1=x_{4,6}=\dot{x}_{1,3}$). Consequently, subsystem Σ_1 is differentially flat.

For subsystem Σ_2 the flat output is $Y_2=x_{4,6}$. Considering that $x_{1,3}$ is a coefficients vector and solving for the real control input u one has

$$u=g_{4,6}(x_{1,3},x_{4,6})^{-1}[\dot{x}_{4,6}-f_{4,6}(x_{1,3},x_{4,6})] \tag{54}$$

which signifies that u is a differential function of $Y_2=x_{4,6}$. Consequently, subsystem Σ_2 is differentially flat.

The proof of differential flatness for subsystems Σ_1 and Σ_2 shows also that these subsystems are input-output linearizable and that they can be controlled through flatness-based control that inverts their dynamics as it is commonly done for input-output linearized systems.

Indeed, for subsystem Σ_1 of Eq. (51) the stabilizing feedback control is taken to be:

$$v_1=g_{1,3}(x_{1,3})^{-1}[\dot{x}_{1,3}^d-f_{1,3}(x_{1,3})-K_1(x_{1,3}-x_{1,3}^d))] \tag{55}$$

where $x_{1,3}^d$ is the reference setpoint for subsystem Σ_1 and matrix $K_1>0$ is a diagonal matrix $K_1\in R^{3\times3}$ with positive diagonal elements $k_{1,ii}>0$ for $i=1,2,3$. The virtual control $v_1=x_{4,6}$ becomes reference setpoint $x_{4,6}^d$ for subsystem Σ_2.

For subsystem Σ_2 of Eq. (52) the stabilizing feedback control is taken to be:

$$u=g_{4,6}(x_{1,3},x_{4,6})^{-1}\\[\dot{x}_{4,6}^d-f_{4,6}(x_{1,3},x_{4,6})-K_2(x_{4,6}-x_{4,6}^d))] \tag{56}$$

where $x_{4,6}^d$ is the reference setpoint for subsystem Σ_2 and matrix $K_2>0$ is a diagonal matrix $K_2\in R^{3\times3}$ with positive diagonal elements $k_{2,ii}>0$ for $i=1,2,3$. The following tracking error variables are defined next: $e_{1,3}=x_{1,3}-x_{1,3}^d$ and $e_{4,6}=x_{4,6}-x_{4,6}^d$.

By substituting the control of Eq. (55) into Eq. (51) one obtains

$$\begin{aligned}&\dot{x}_{1,3}=f_{1,3}(x_{1,3})+g_{1,3}(x_{1,3})g_{1,3}(x_{1,3})^{-1}\\&[\dot{x}_{1,3}^d-f_{1,3}(x_{1,3})-K_1(x_{1,3}-x_{1,3}^d))]\Rightarrow\\&(\dot{x}_{1,3}-\dot{x}_{1,3}^d)+K_1(x_{1,3}-x_{1,3}^d)\Rightarrow\\&\dot{e}_{1,3}+K_1e_{1,3}=0\Rightarrow\\&\lim_{t\to\infty}e_{1,3}=0\Rightarrow\lim_{t\to\infty}x_{1,3}=x_{1,3}^d\end{aligned} \tag{57}$$

By substituting the control of Eq. (56) into Eq. (52) one obtains

$$\begin{aligned}&\dot{x}_{4,6}=f_{4,6}(x_{1,3},x_{4,6})+g_{4,6}(x_{1,3},x_{4.6})g_{4,6}(x_{1,3},x_{4,6})^{-1}\\&[\dot{x}_{4,6}^d-f_{4,6}(x_{1,3},x_{4,6})-K_2(x_{4,6}-x_{4,6}^d))]\Rightarrow\\&(\dot{x}_{4,6}-\dot{x}_{4,6}^d)+K_2(x_{4,6}-x_{4,6}^d)\Rightarrow\\&\dot{e}_{4,6}+K_2e_{4,6}=0\Rightarrow\\&\lim_{t\to\infty}e_{4,6}=0\Rightarrow\\&\lim_{t\to\infty}x_{4,6}=x_{4,6}^d\end{aligned} \tag{58}$$

Consequently, all state variables of the dynamic model of the 3-wheel omnidirectional mobile robot converge to the associated setpoints and the system is globally asymptotically stable.

The global stability properties of flatness-based control in successive loops for the dynamic model of the 3-wheel omnidirectional mobile robot can be also proven through Lyapunov analysis. The following Lyapunov function is defined:

$$V=\frac{1}{2}[e_{1,3}^Te_{1,3}+e_{4,6}^Te_{4,6}] \tag{59}$$

By differentiating the Lyapunov function of Eq. (59) in time one obtains

$$\dot{V} = \frac{1}{2}2[e_{1,3}^T \dot{e}_{1,3} + e_{4,6}^T \dot{e}_{4,6}] \quad (60)$$

By substituting in Eq. (60) the tracking error dynamics proven in Eq. (57) and Eq. (58) one obtains

$$\dot{V} = -[e_{1,3}^T K_1 e_{1,3} + e_{4,6}^T K_2 e_{4,6}] \quad (61)$$

Therefore, it holds that

$$\dot{V} < 0 \; \forall \; e_{1,3} \neq 0, \; e_{4,6} \neq 0 \quad (62)$$

while $\dot{V} = 0$ if and only if $e_{1,3} = 0$ and $e_{4,6} = 0$. Thus, $\dot{V}$ remains negative and V is a strictly diminishing function which converges asymptotically to 0. Thus it holds

$$\begin{matrix} lim_{t\to\infty} e_{1,3} = 0 \Rightarrow lim_{t\to\infty} x_{1,3} = x_{1,3}^d \\ lim_{t\to\infty} e_{4,6} = 0 \Rightarrow lim_{t\to\infty} x_{4,6} = x_{4,6}^d \end{matrix} \quad (63)$$

It is also proven that the convergence of the tracking error to the zero equilibrium is exponential. The Lyapunov function of the control loop is written as:

$$V = \frac{1}{2}[\sum_{i=1}^{3} e_i^2 + \sum_{j=4}^{6} e_j^2] \quad (64)$$

where $e_i \; i = 1, \cdots, 3$ are the tracking errors for the state variables of the mobile robot associated with position and orientation and $e_j \; j = 4, \cdots, 6$ are the tracking errors for the state variables of the mobile robot associated with linear and angular velocities. Equivalently, the first-order time-derivative of the Lyapunov function is written as

$$\dot{V} = -[\sum_{i=1}^{3} k_{1,i} e_i^2 + \sum_{j=4}^{6} k_{2,j} e_j^2] \quad (65)$$

where $k_{1,i} > 0 \; i = 1, \cdots, 3$ are the diagonal elements of gain matrix K_1 and $k_{2,j} > 0 \; j = 4, \cdots, 6$ are the diagonal elements of gain matrix K_2. By denoting the minimum of the above-noted elements of the feedback gain matrices as k_{min}, that is

$$k_{min} = min\{k_{1,i} : \; i = 1, \cdots, 3 \text{ and } k_{2,j} : \; j = 4, \cdots, 6\} \quad (66)$$

and using Eq. (65) one obtains that

$$\begin{matrix} \dot{V} \leq -k_{min}[\sum_{i=1}^{4} e_i^2 + \sum_{j=4}^{6} e_j^2] \\ \Rightarrow \dot{V} \leq -2k_{min} V \Rightarrow \dot{V} + 2k_{min} V \leq 0 \end{matrix} \quad (67)$$

From Eq. (67) one can demonstrate the exponential convergence of the Lyapunov function V to 0.

Finally, a diagram with the implementation stages of multi-loop flatness-based control method is given in Figure 3.

Once the state-space model of the system has been separated into chained subsystems which individually satisfy the differential flatness property, flatness-based control is implemented at each time-step through the following steps: (i) the state vector of the subsequent $(i + 1)$-th subsystem becomes virtual control input to the preceding i-th subsystem, (ii) Equivalently, the virtual control input of the preceding i-th subsystem becomes setpoint for the subsequent $(i + 1)$-th subsystem, (iii) the value of the virtual control input for each subsystem is computed by inverting the dynamics of this subsystem and by selecting feedback gains which allow for eliminating the associated local tracking error, (iv) the real control input is computed from the last subsystem by inverting again the dynamics of this subsystem (v) the real control input makes implicitly use of the virtual control inputs of all preceding subsystems. Its stabilizing effects appear by tracing the subsystems of the state-space model backwards from the last to the first one.

5. Simulation Tests

5.1. Results on Nonlinear Optimal Control for the 3-DOF Omnidirectional Robot

The proposed nonlinear optimal control method for the 3-wheel omnidirectional mobile robot has been tested and its performance has been further confirmed through simulation tests. To implement the nonlinear optimal control method the algebraic Riccati equation of Eq. (39) had to be repetitively solved at each time-step of the control algorithm, with the use of Matlab's function *aresolv()*. The Jacobian matrices of the system were also updated at each sampling instance. Indicative values about the parameters of the mobile robot were as follows: $n = 0.5$, $r = 0.1m$, $m = 10kg$, $I_o = 0.05kg{\cdot}m^2$, $k_t = 0.01$, $k_b = 0.01$, $I_v = 4kg{\cdot}m^2$, $L_o = 0.5m$, $b_o = 0.01$, $R_a = 0.1\Omega$, $d_1 = 0.02$, $d_2 = 0.02$, $d_3 = 0.02$. The obtained results are depicted in Figure 4 to Figure 19. The measurement units for the cartesian coordinates of the robotic vehicle were in meters (m) and for its rotation angles were in radians (rad). The measurement units for linear velocity variables were m/sec while angular velocity variables were measured in rad/sec. The real values of the state variables of the 3-wheel omnidirectional mobile robot are depicted in blue, their estimated values which have been provided by the H-infinity Kalman Filter are plotted in green while the associated reference setpoints are printed in red. The simulation results have shown that the nonlinear optimal control scheme achieves fast and accurate tracking of setpoints under moderate variations of the control inputs. The obtained results contain 2D diagrams are given about the tracking of reference trajectories by the center-of-gravity of the robotic vehicle.

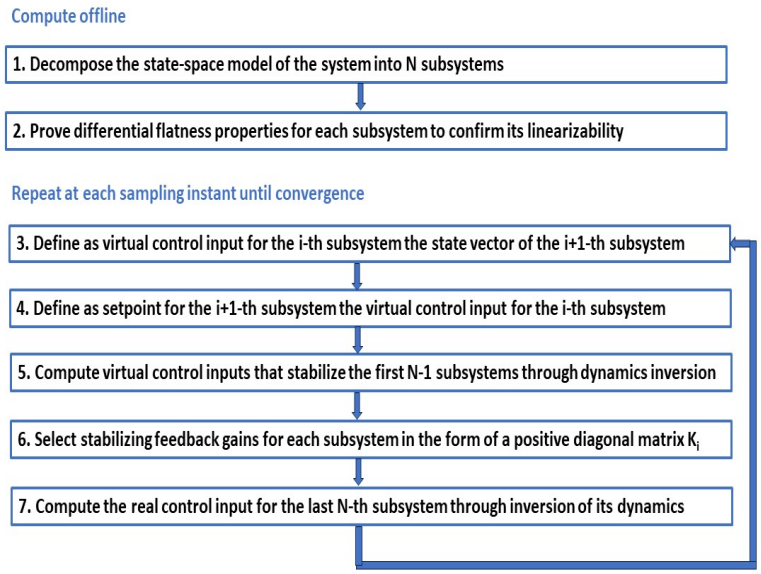

Figure 3. Diagram with the implementation stages of multi-loop flatness-based control of the three-wheel omnidirectional mobile robot [Source: Authors' own work]

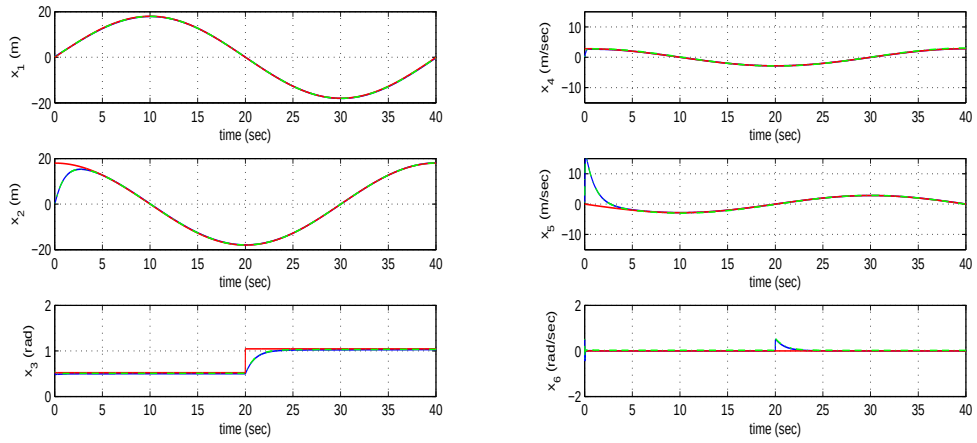

Figure 4. Nonlinear optimal control - Tracking of setpoint 1 for the 3-wheel omnidirectional mobile robot (a) convergence of state variables x_1 to x_3 to their reference setpoints (red line: setpoint, blue line: real value, green line: estimated value), (b) convergence of state variables x_4 to x_6 to their reference setpoints (red line: setpoint, blue line: real value, green line: estimated value) [Source: Authors' own work]

The transient performance of the control method depends mainly of gains r, ρ and on gain matrix Q which appear in the Riccati equation of Eq. (39). Actually, by assigning small values to r one can achieve elimination of the state vector's tracking error, while by assigning relatively large values to the diagonal elements of matrix Q one can achieve fast convergence of state variables to setpoints. Moreover, the smallest value of ρ for which one can obtain a valid solution for the above-noted Riccati equation (in the form of positive-definite and symmetric matrix P) is the one that provides the control loop with maximum robustness. The nonlinear optimal control method results into minimization of energy dispersion by the actuators of the 3-wheel omnidirectional mobile robot, thus increasing the autonomy and operational capacity of the autonomous vehicle. The method exhibits global (and not local) stability properties as it is confirmed by its ability to track time-varying and abruptly changing setpoints.

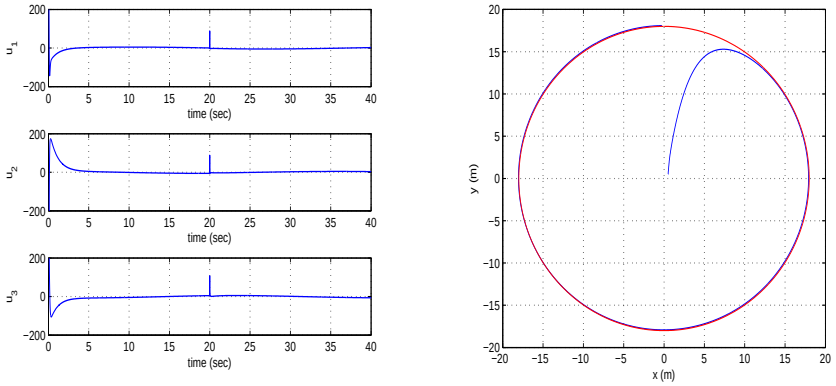

(a) **(b)**

Figure 5. Nonlinear optimal control - Tracking of setpoint 1 for the 3-wheel omnidirectional mobile robot (a) variations of the control inputs u_1 to u_3 (b) tracking of the reference trajectory by the center of gravity of the mobile robot in the 2D xy plane [Source: Authors' own work]

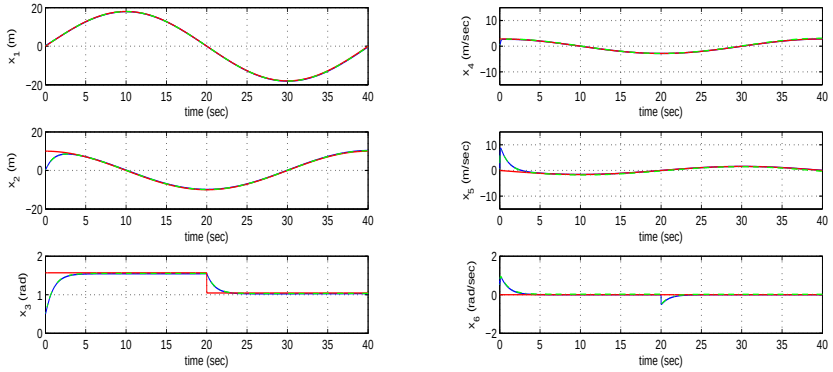

(a) **(b)**

Figure 6. Nonlinear optimal control - Tracking of setpoint 2 for the 3-wheel omnidirectional mobile robot (a) convergence of state variables x_1 to x_3 to their reference setpoints (red line: setpoint, blue line: real value, green line: estimated value), (b) convergence of state variables x_4 to x_6 to their reference setpoints (red line: setpoint, blue line: real value, green line: estimated value) [Source: Authors' own work]

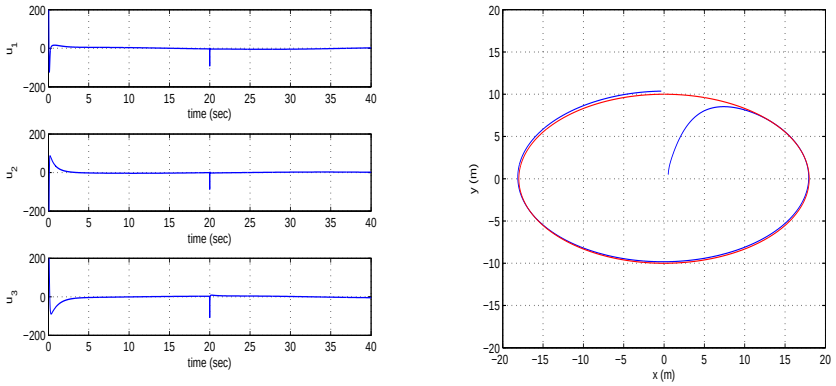

(a) **(b)**

Figure 7. Nonlinear optimal control - Tracking of setpoint 2 for the 3-wheel omnidirectional mobile robot (a) variations of the control inputs u_1 to u_3 (b) tracking of the reference trajectory by the center of gravity of the mobile robot in the 2D xy plane [Source: Authors' own work]

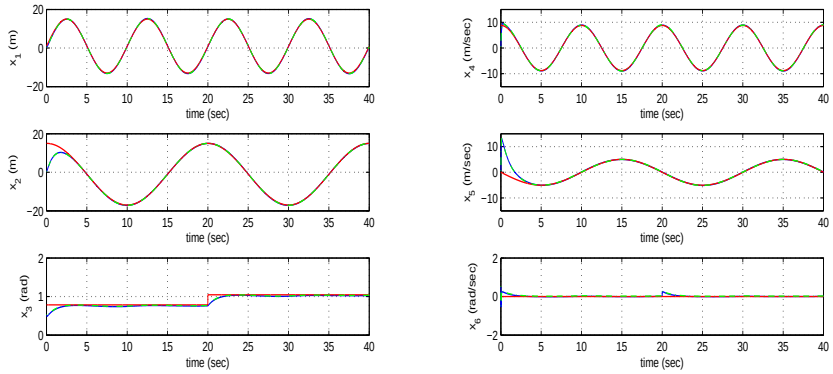

(a) **(b)**

Figure 8. Nonlinear optimal control - Tracking of setpoint 3 for the 3-wheel omnidirectional mobile robot (a) convergence of state variables x_1 to x_3 to their reference setpoints (red line: setpoint, blue line: real value, green line: estimated value), (b) convergence of state variables x_4 to x_6 to their reference setpoints (red line: setpoint, blue line: real value, green line: estimated value) [Source: Authors' own work]

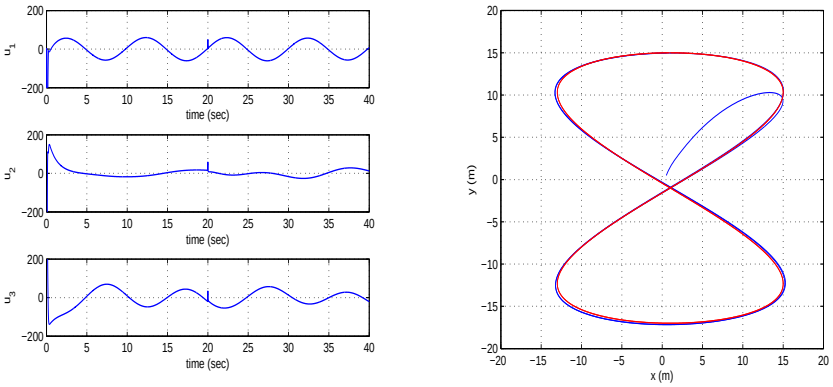

(a) **(b)**

Figure 9. Nonlinear optimal control - Tracking of setpoint 3 for the 3-wheel omnidirectional mobile robot (a) variations of the control inputs u_1 to u_3 (b) tracking of the reference trajectory by the center of gravity of the mobile robot in the 2D xy plane [Source: Authors' own work]

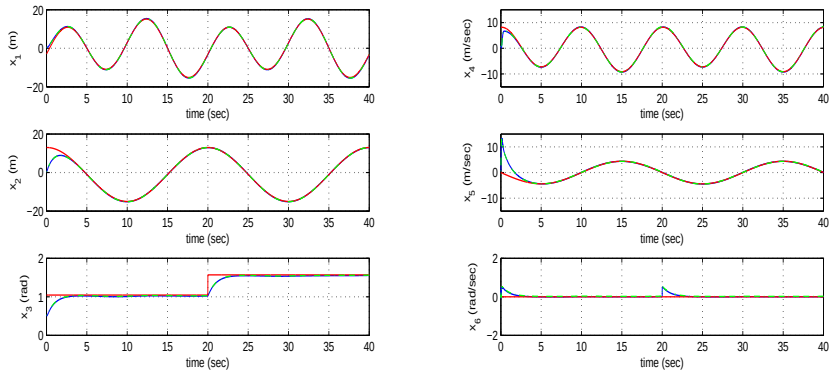

(a) **(b)**

Figure 10. Nonlinear optimal control - Tracking of setpoint 4 for the 3-wheel omnidirectional mobile robot (a) convergence of state variables x_1 to x_3 to their reference setpoints (red line: setpoint, blue line: real value, green line: estimated value), (b) convergence of state variables x_4 to x_6 to their reference setpoints (red line: setpoint, blue line: real value, green line: estimated value) [Source: Authors' own work]

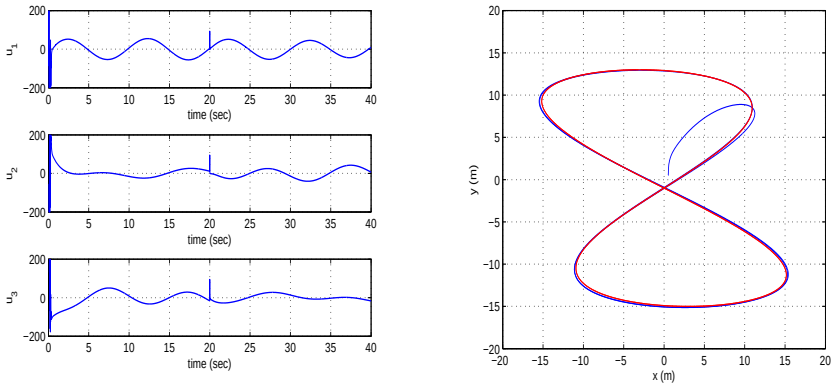

(a) **(b)**

Figure 11. Nonlinear optimal control - Tracking of setpoint 4 for the 3-wheel omnidirectional mobile robot (a) variations of the control inputs u_1 to u_3 (b) tracking of the reference trajectory by the center of gravity of the mobile robot in the 2D xy plane [Source: Authors' own work]

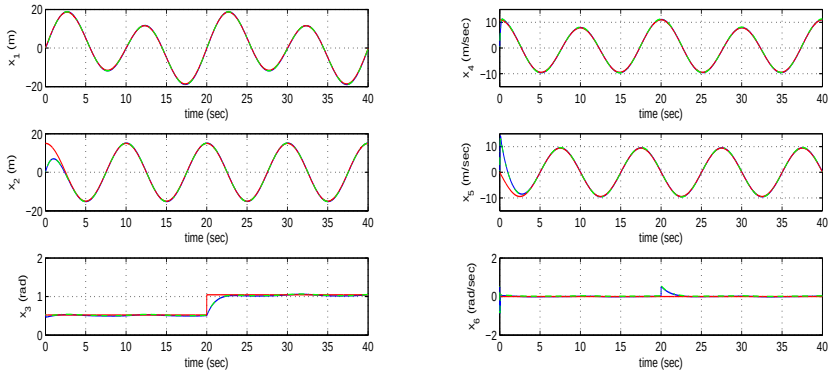

(a) **(b)**

Figure 12. Nonlinear optimal control - Tracking of setpoint 5 for the 3-wheel omnidirectional mobile robot (a) convergence of state variables x_1 to x_3 to their reference setpoints (red line: setpoint, blue line: real value, green line: estimated value), (b) convergence of state variables x_4 to x_6 to their reference setpoints (red line: setpoint, blue line: real value, green line: estimated value) [Source: Authors' own work]

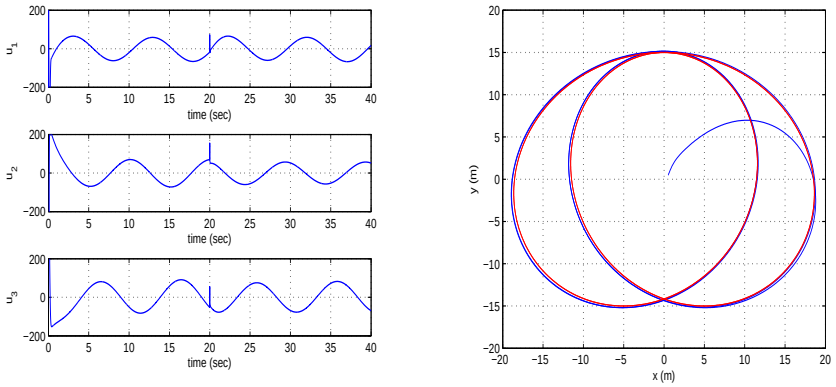

(a) **(b)**

Figure 13. Nonlinear optimal control - Tracking of setpoint 5 for the 3-wheel omnidirectional mobile robot (a) variations of the control inputs u_1 to u_3 (b) tracking of the reference trajectory by the center of gravity of the mobile robot in the 2D xy plane [Source: Authors' own work]

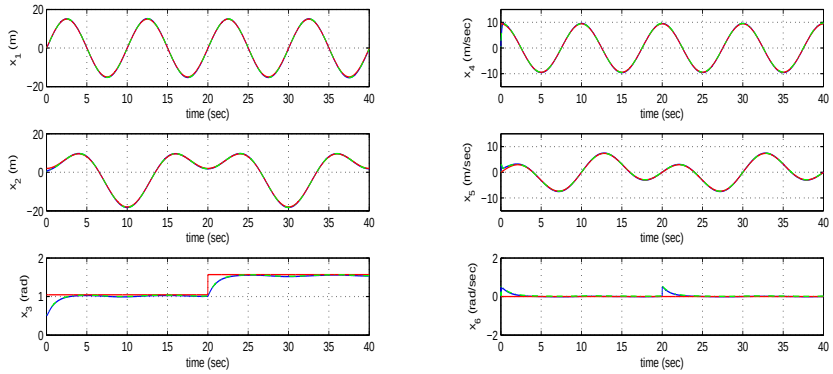

(a) **(b)**

Figure 14. Nonlinear optimal control - Tracking of setpoint 6 for the 3-wheel omnidirectional mobile robot (a) convergence of state variables x_1 to x_3 to their reference setpoints (red line: setpoint, blue line: real value, green line: estimated value), (b) convergence of state variables x_4 to x_6 to their reference setpoints (red line: setpoint, blue line: real value, green line: estimated value) [Source: Authors' own work]

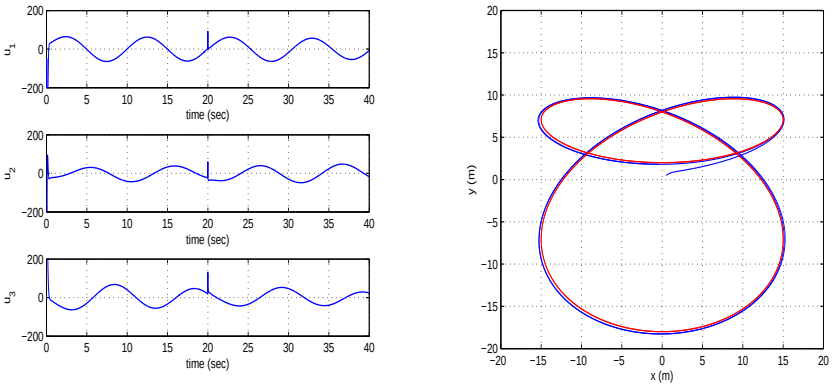

(a) **(b)**

Figure 15. Nonlinear optimal control - Tracking of setpoint 6 for the 3-wheel omnidirectional mobile robot (a) variations of the control inputs u_1 to u_3 (b) tracking of the reference trajectory by the center of gravity of the mobile robot in the 2D xy plane [Source: Authors' own work]

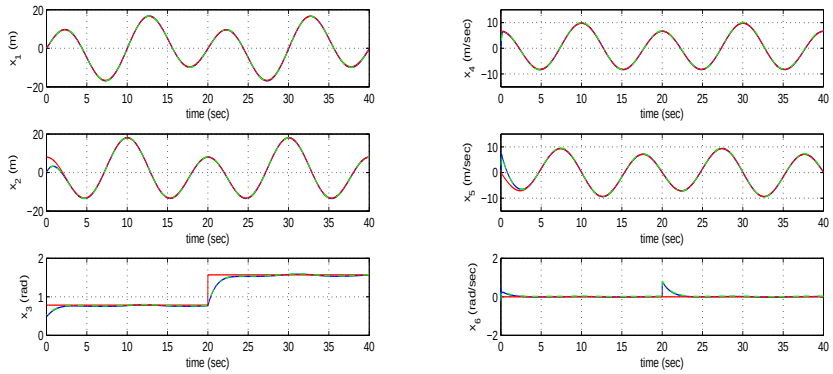

(a) **(b)**

Figure 16. Nonlinear optimal control - Tracking of setpoint 7 for the 3-wheel omnidirectional mobile robot (a) convergence of state variables x_1 to x_3 to their reference setpoints (red line: setpoint, blue line: real value, green line: estimated value), (b) convergence of state variables x_4 to x_6 to their reference setpoints (red line: setpoint, blue line: real value, green line: estimated value) [Source: Authors' own work]

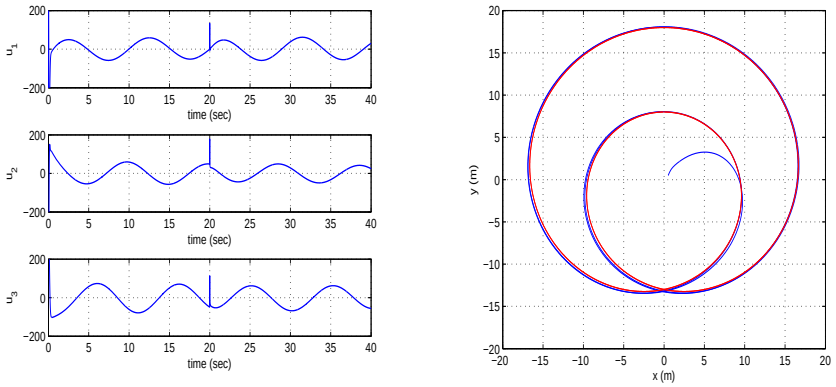

(a) **(b)**

Figure 17. Nonlinear optimal control - Tracking of setpoint 7 for the 3-wheel omnidirectional mobile robot (a) variations of the control inputs u_1 to u_3 (b) tracking of the reference trajectory by the center of gravity of the mobile robot in the 2D xy plane [Source: Authors' own work]

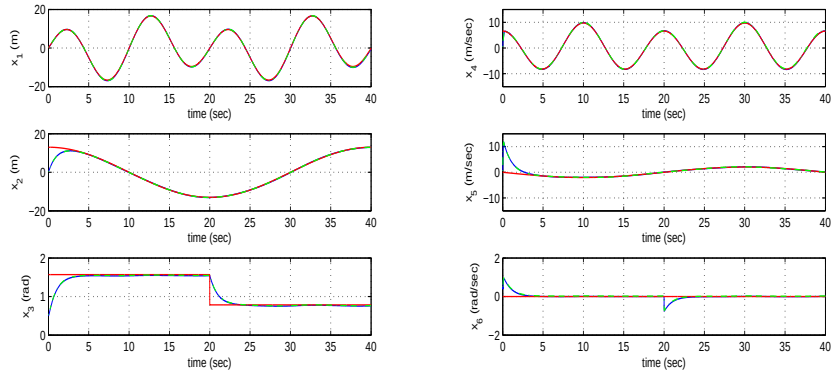

(a) **(b)**

Figure 18. Nonlinear optimal control - Tracking of setpoint 8 for the 3-wheel omnidirectional mobile robot (a) convergence of state variables x_1 to x_3 to their reference setpoints (red line: setpoint, blue line: real value, green line: estimated value), (b) convergence of state variables x_4 to x_6 to their reference setpoints (red line: setpoint, blue line: real value, green line: estimated value) [Source: Authors' own work]

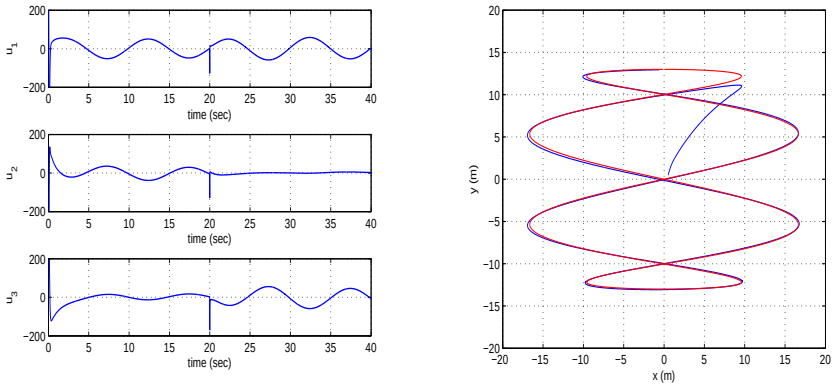

(a) **(b)**

Figure 19. Nonlinear optimal control - Tracking of setpoint 8 for the 3-wheel omnidirectional mobile robot (a) variations of the control inputs u_1 to u_3 (b) tracking of the reference trajectory by the center of gravity of the mobile robot in the 2D xy plane [Source: Authors' own work]

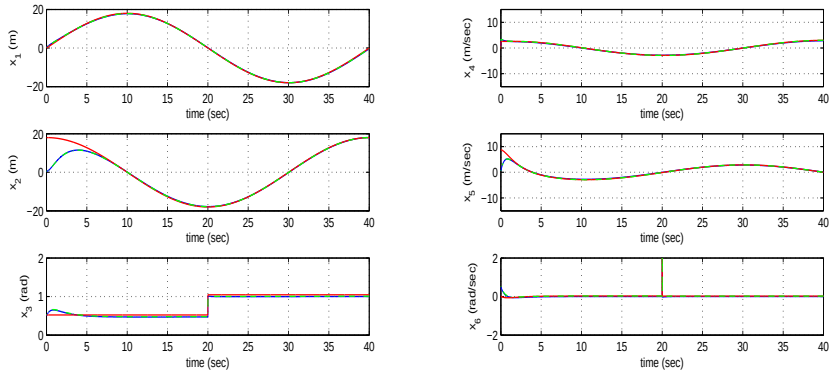

(a) **(b)**

Figure 20. Multi-loop flatness-based control - Tracking of setpoint 1 for the 3-wheel omnidirectional mobile robot (a) convergence of state variables x_1 to x_3 to their reference setpoints (red line: setpoint, blue line: real value, green line: estimated value), (b) convergence of state variables x_4 to x_6 to their reference setpoints (red line: setpoint, blue line: real value, green line: estimated value) [Source: Authors' own work]

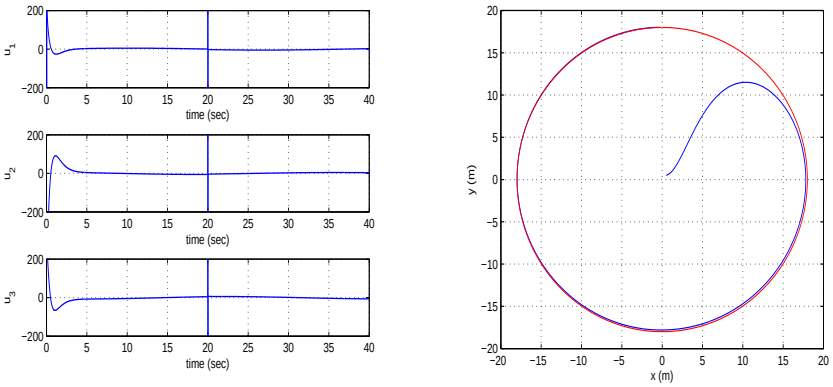

(a) **(b)**

Figure 21. Multi-loop flatness-based control - Tracking of setpoint 1 for the 3-wheel omnidirectional mobile robot (a) variations of the control inputs u_1 to u_3 (b) tracking of the reference trajectory by the center of gravity of the mobile robot in the 2D xy plane [Source: Authors' own work]

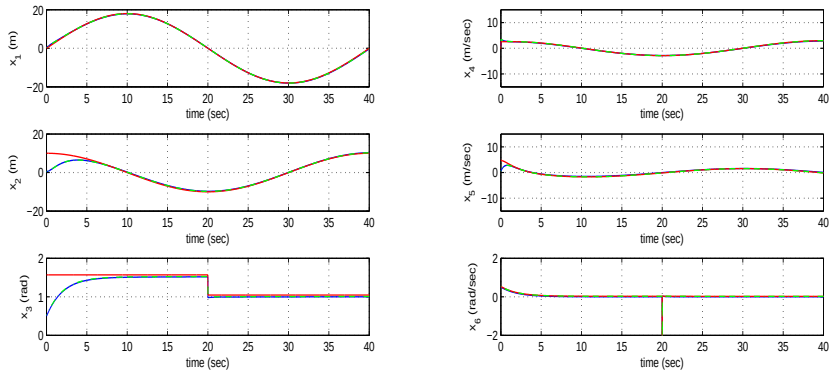

(a) **(b)**

Figure 22. Multi-loop flatness-based control - Tracking of setpoint 2 for the 3-wheel omnidirectional mobile robot (a) convergence of state variables x_1 to x_3 to their reference setpoints (red line: setpoint, blue line: real value, green line: estimated value), (b) convergence of state variables x_4 to x_6 to their reference setpoints (red line: setpoint, blue line: real value, green line: estimated value) [Source: Authors' own work]

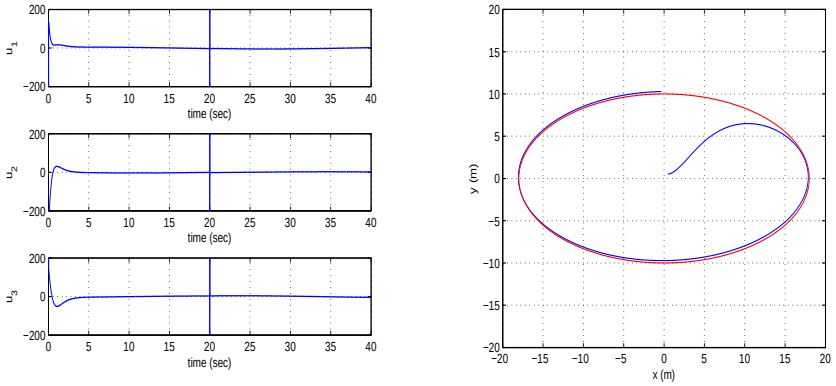

(a) **(b)**

Figure 23. Multi-loop flatness-based control - Tracking of setpoint 2 for the 3-wheel omnidirectional mobile robot (a) variations of the control inputs u_1 to u_3 (b) tracking of the reference trajectory by the center of gravity of the mobile robot in the 2D xy plane [Source: Authors' own work]

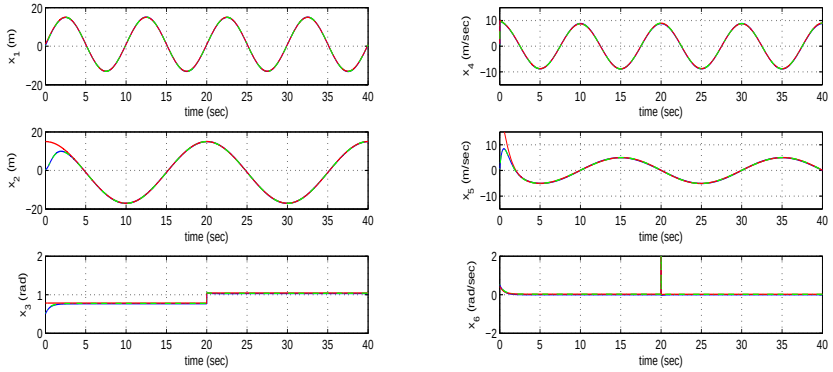

(a) **(b)**

Figure 24. Multi-loop flatness-based control - Tracking of setpoint 3 for the 3-wheel omnidirectional mobile robot (a) convergence of state variables x_1 to x_3 to their reference setpoints (red line: setpoint, blue line: real value, green line: estimated value), (b) convergence of state variables x_4 to x_6 to their reference setpoints (red line: setpoint, blue line: real value, green line: estimated value) [Source: Authors' own work]

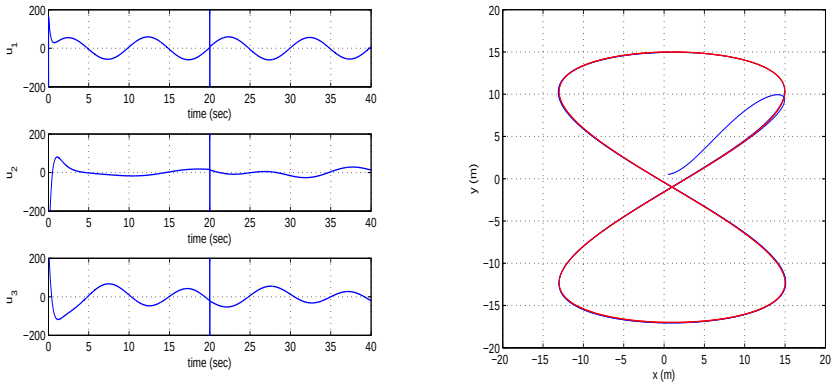

(a) **(b)**

Figure 25. Multi-loop flatness-based control - Tracking of setpoint 3 for the 3-wheel omnidirectional mobile robot (a) variations of the control inputs u_1 to u_3 (b) tracking of the reference trajectory by the center of gravity of the mobile robot in the 2D xy plane [Source: Authors' own work]

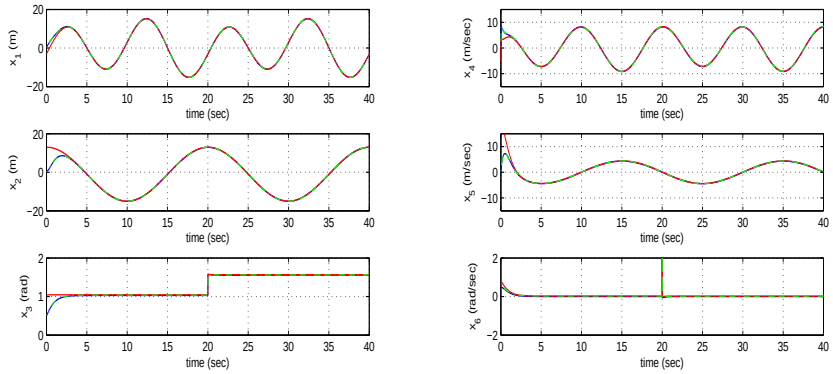

(a) **(b)**

Figure 26. Multi-loop flatness-based control - Tracking of setpoint 4 for the 3-wheel omnidirectional mobile robot (a) convergence of state variables x_1 to x_3 to their reference setpoints (red line: setpoint, blue line: real value, green line: estimated value), (b) convergence of state variables x_4 to x_6 to their reference setpoints (red line: setpoint, blue line: real value, green line: estimated value) [Source: Authors' own work]

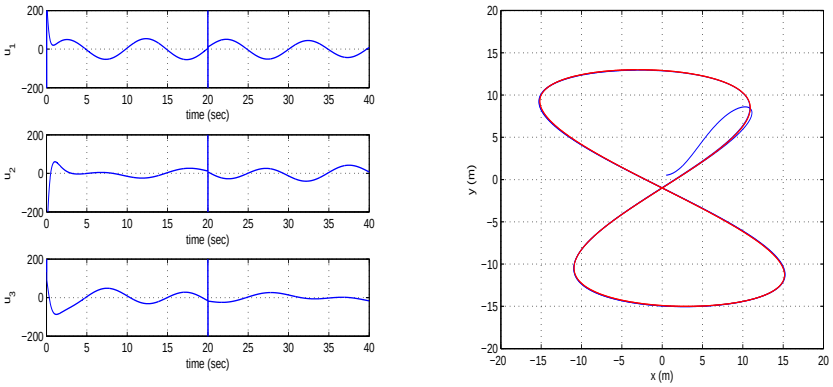

(a) **(b)**

Figure 27. Multi-loop flatness-based control - Tracking of setpoint 4 for the 3-wheel omnidirectional mobile robot (a) variations of the control inputs u_1 to u_3 (b) tracking of the reference trajectory by the center of gravity of the mobile robot in the 2D xy plane [Source: Authors' own work]

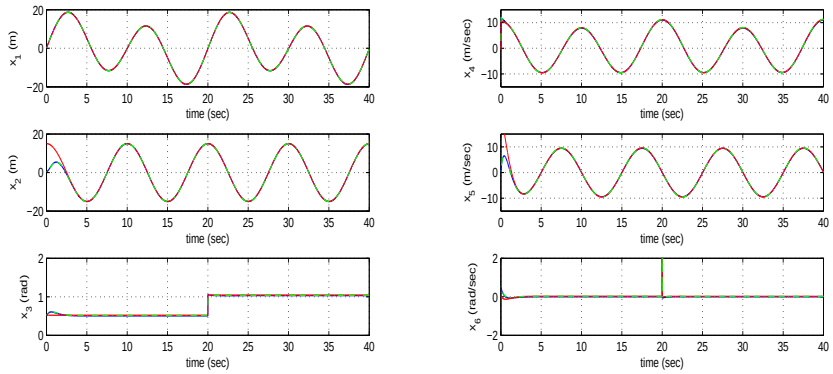

(a) **(b)**

Figure 28. Multi-loop flatness-based control - Tracking of setpoint 5 for the 3-wheel omnidirectional mobile robot (a) convergence of state variables x_1 to x_3 to their reference setpoints (red line: setpoint, blue line: real value, green line: estimated value), (b) convergence of state variables x_4 to x_6 to their reference setpoints (red line: setpoint, blue line: real value, green line: estimated value) [Source: Authors' own work]

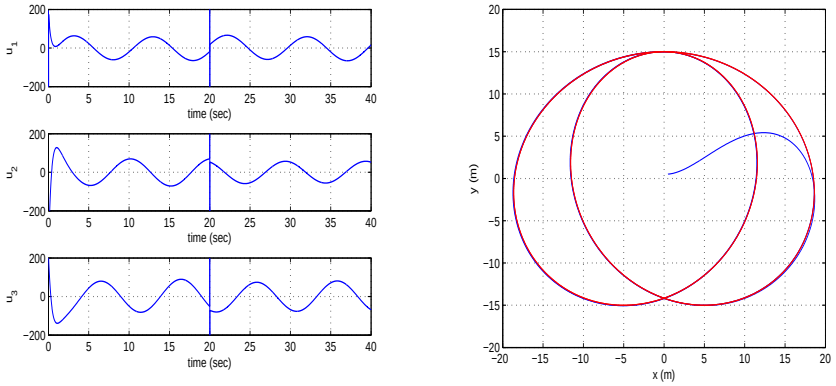

(a) **(b)**

Figure 29. Multi-loop flatness-based control - Tracking of setpoint 5 for the 3-wheel omnidirectional mobile robot (a) variations of the control inputs u_1 to u_3 (b) tracking of the reference trajectory by the center of gravity of the mobile robot in the 2D xy plane [Source: Authors' own work]

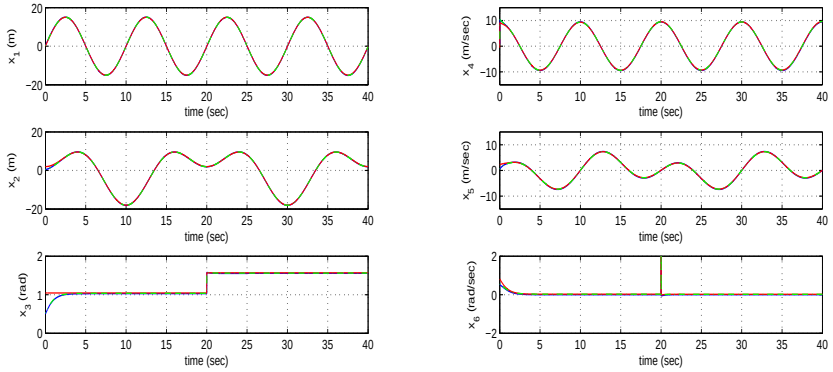

(a) **(b)**

Figure 30. Multi-loop flatness-based control - Tracking of setpoint 6 for the 3-wheel omnidirectional mobile robot (a) convergence of state variables x_1 to x_3 to their reference setpoints (red line: setpoint, blue line: real value, green line: estimated value), (b) convergence of state variables x_4 to x_6 to their reference setpoints (red line: setpoint, blue line: real value, green line: estimated value) [Source: Authors' own work]

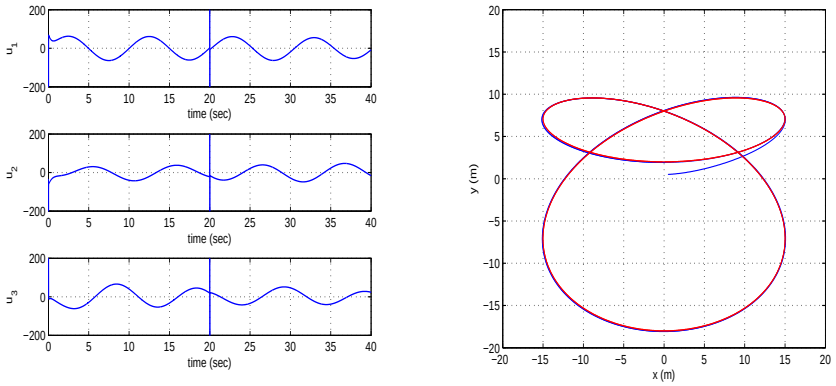

(a) **(b)**

Figure 31. Multi-loop flatness-based control - Tracking of setpoint 6 for the 3-wheel omnidirectional mobile robot (a) variations of the control inputs u_1 to u_3 (b) tracking of the reference trajectory by the center of gravity of the mobile robot in the 2D xy plane [Source: Authors' own work]

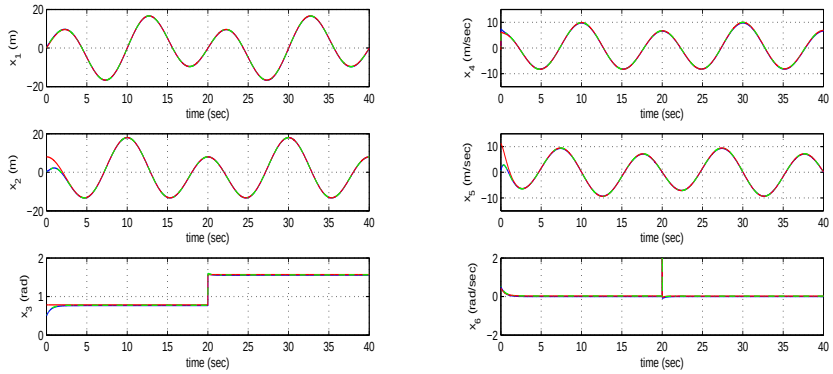

(a) **(b)**

Figure 32. Multi-loop flatness-based control - Tracking of setpoint 7 for the 3-wheel omnidirectional mobile robot (a) convergence of state variables x_1 to x_3 to their reference setpoints (red line: setpoint, blue line: real value, green line: estimated value), (b) convergence of state variables x_4 to x_6 to their reference setpoints (red line: setpoint, blue line: real value, green line: estimated value) [Source: Authors' own work]

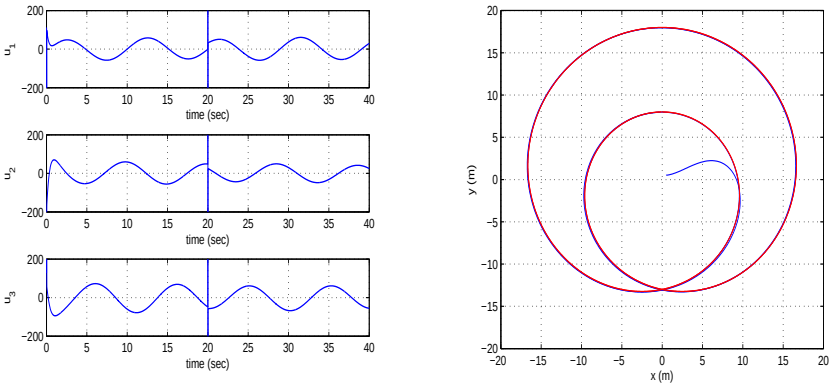

(a) **(b)**

Figure 33. Multi-loop flatness-based control - Tracking of setpoint 7 for the 3-wheel omnidirectional mobile robot (a) variations of the control inputs u_1 to u_3 (b) tracking of the reference trajectory by the center of gravity of the mobile robot in the 2D xy plane [Source: Authors' own work]

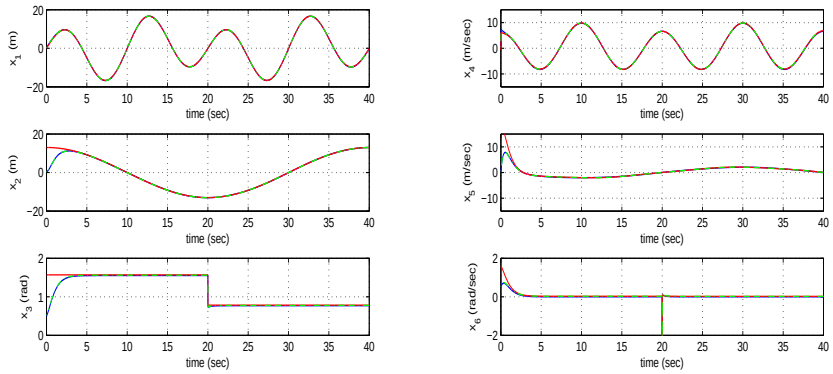

(a) **(b)**

Figure 34. Multi-loop flatness-based control - Tracking of setpoint 8 for the 3-wheel omnidirectional mobile robot (a) convergence of state variables x_1 to x_3 to their reference setpoints (red line: setpoint, blue line: real value, green line: estimated value), (b) convergence of state variables x_4 to x_6 to their reference setpoints (red line: setpoint, blue line: real value, green line: estimated value) [Source: Authors' own work]

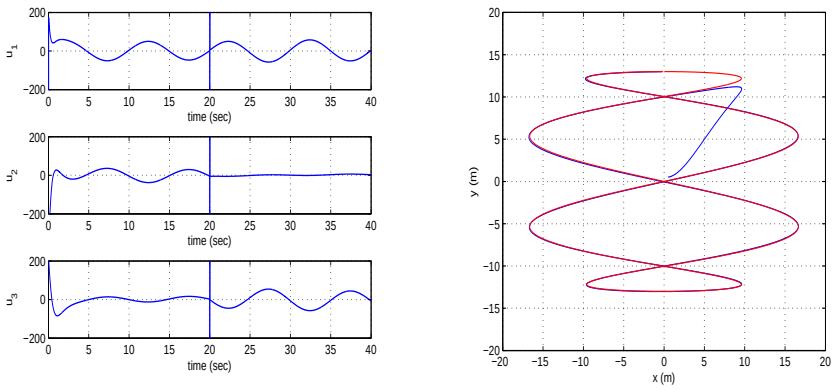

(a) **(b)**

Figure 35. Multi-loop flatness-based control - Tracking of setpoint 8 for the 3-wheel omnidirectional mobile robot (a) variations of the control inputs u_1 to u_3 (b) tracking of the reference trajectory by the center of gravity of the mobile robot in the 2D xy plane [Source: Gerasimos own work]

5.2. Results on Multi-loop Flatness-based Control for the 3-DOF Omnidirectional Robot

Results about the tracking accuracy and the speed of convergence to setpoints of the flatness-based control method in successive-loops, in the case of the 3-wheel omnidirectional mobile robot, are shown in Figure 20 to Figure 35. The measurement units for the cartesian coordinates of the robotic vehicle were in meters (m) and for its orientation angle were in radians (rad). The measurement units for linear velocity variables were m/sec while angular velocity variables were measured in rad/sec.

The real values of the state variables of the autonomous robotic vehicle are depicted in blue, their estimated values which have been provided by the H-infinity Kalman Filter are plotted in green while the associated reference setpoints are printed in red. The simulation results have shown that flatness-based control in successive loops achieves precise tracking of setpoints under moderate variations of the control inputs. Once again, 2D diagrams are given about the tracking of reference trajectories by the center-of-gravity of the mobile robot.

It can be noticed again, that under this control scheme one achieves fast and precise tracking of reference setpoints for all state variables of the dynamic model of the 3-wheel omnidirectional mobile robot without changes of state variables and without state space-model transformations. It is noteworthy, that through the stages of this method one solves also the setpoints definition problem for all state variables of the autonomous robotic vehicle. Actually, the selection of setpoints for the state variables of the first subsystem in the chained state-space form is unconstrained.

On the other side by taking the state variables of the subsequent subsystem to be virtual control inputs for the preceding subsystem one can find also the setpoints of the subsequent subsystem (the state variables of the subsequent subsystem should converge to the virtual control input that stabilizes its preceding subsystem). The speed of convergence of the state variables of the dynamic model of the robotic vehicle under flatness-based control implemented in successive loops is determined by the selection of values for the diagonal gain matrices K_1, K_2.

6. Conclusion

The aim of the present article has been to develop novel nonlinear control methods for the dynamic model of the 3-wheel omnidirectional mobile robot which do not need changes of state variables or complicated state-space model transformations. To this end the following two control methods have been developed and tested (i) nonlinear optimal control, (ii) flatness-based control in successive loops. In the nonlinear optimal control method the dynamic model of the omnidirectional mobile robot has undergone first approximate linearization with the use of first-order Taylor series expansion and through the computation of the associated Jacobian matrices. This linearization process was taking place at each sampling instant around a time-varying operating point which was defined by the present value of the system's state vector and by the last sampled value of the control inputs vector. For the linearized model of the mobile robot an H-infinity feedback controller has been designed. The H-infinity control method signifies a min-max differential game between the control and the disturbance inputs and achieves solution of the associated optimal control problem under model uncertainty and exogenous perturbations.

To compute the gains of the H-infinity controller an algebraic Riccati equation had to be repetitively solved at each sampling period. The global stability properties of the nonlinear optimal control method have been proven through Lyapunov analysis.

In the multi-loop flatness-based control method, the dynamic model of the 3-wheel omnidirectional mobile robot was separated into subsystems connected in chained form. The state vector of the subsequent (i+1-th) subsystem was a virtual control input for the preceding (i-th) subsystem. Moreover, the virtual control input for the preceding (i-th) subsystem was the setpoint for the subsequent (i+1-th) subsystem. It was proven that all subsystems in this chained state-space structure were differentially flat. Thus it was confirmed that they were input-output linearizable and that a stabilizing flatness-based controller could be designed for each one of them by inverting their dynamics, as it is commonly done for input-output linearized systems. The real control inputs of the omnidirectional mobile robot were computed from the last subsystem in this chained state-space structure. In this computation the virtual control inputs of the preceding subsystems had to be traced backwards, from the last to the first subsystem, within each sampling period. The global stability properties of the multi-loop flatness-based control scheme were also proven through Lyapunov analysis.

AUTHORS

Gerasimos Rigatos – Unit of Industrial Automation, Industrial Systems Institute, 26504, Rion Patras, Greece, e-mail: grigat@ieee.org.

Masoud Abbaszadeh – Dept. of ECS Engineering, Rensselaer Polytechnic Institute, 12065, Troy, New York USA, e-mail: masouda@ualberta.ca.

References

[1] C. Ren, X. Li, X. Yiang and S. Ma, *Extended state observer-based sliding-mode control of an omnidirectional mobile robot with friction compensation*, IEEE Transactions on Industrial Electronics, vol. 66, no. 17, pp. 9580-9489, 2019.

[2] H. Kim and B.K. Kim, *Online minimum energy trajectory planning and control on a straight-line path for three-wheeled omnidirectional mobile robots*, IEEE Transactions on Industrial Electronics, vol. 61, no. 9, pp. 4721-4779, 2014.

[3] C. Ren, Y. Ding and S. Ma, *A structure improved extended state observer-based control with application to an omnidirectional mobile robot*, ISA Transactions, Elsevier, vol. 101, pp. 335-345, 2020.

[4] J.C. Lins Barreto, A.G. Scolari Conceicao, C.E.T. Dorea, L. Martinez and E.R. de Pieri, *Design and implementation of Model Predictive Control with friction compensation of an omnidirectional mobile robot*, IEEE/ASME Transactions on Mechatronics, vol. 19, no. 2, pp. 462-476, 2014.

[5] K.B. Kim and B.K. Kim, *Minimum-time trajectory of three-wheel omnidirectional mobile robots following a bounded curvature path with a referenced heading profile*, IEEE Transactions on Robotics, vol. 27, no. 6, pp. 800-808, 2011.

[6] M. El-Sayyah, M.E. Saad and M. Saad, *Enhanced MPC for omnidirectional robot motion tracking using Laguerre functions and non-iterative linearization*, IEEE Access, vol. 10, pp. 118290-118302, 2022.

[7] H.C. Huang, *SoPC based parallel ACO algorithm and its application to optimal motion controller design for intelligent omnidirectional mobile robot*, IEEE Transactions on Industrial Informatics, vol. 9, no. 4, pp. 1828-1835, 2013.

[8] M. Hamaguchi, *Damping and transfer control system with parallel linkage mechanism-based active vibration reducer for omnidirectional wheeled robots*, IEEE/ASME Transactions on Mechatronis, vol. 23, no. 4, pp. 2424-2435, 2019.

[9] T. Kalmar-Nagy, R.D. Andreu and P Ganguly, *Near-optimal dynamic trajectory generation and control of an omnidirectional vehicle*, Robotics and Autonomous Systems, Elsevier, vol. 46, pp. 47-64, 2004.

[10] F. Dong, D. Jin, X. Zhou, and J. Han, *Adaptive robust constraint following control for omnidirectional mobile robot: An indirect approach*, IEEE Access, vol. 9, pp. 8877=8889, 2021.

[11] J. Liu, J. Zhu, R.L. Williams and J. Wu, *Omnidirectional mobile robot controller based on trajectory linearization*, Robotics and Autonomous Systems, Elsevier, vol. 56, pp. 461-479, 2005.

[12] V.T. Dinh, H. Nguyen, S.M. Shin, M.K, Kim, S.B. Kim and G.S. Bynn, *Tracking control of omnidirectional mobile platform with disturbance using diffeential sliding-mode controller*, Journal of Precision Engineering Springer, vol, 19, no,5, pp. 39-48, 2012.

[13] N. Hacen and B. Merdal, *Motion analysis and control of omnidirectional mobile robot*, Journal of Control, Automation and Electrical Systems, Springer, vol. 30, pp. 194-213, 2019.

[14] D.J. Balkom, P.A. Kavathekar and M.T. Mason, *Time-optimal trajectory for an omnidirectional vehicle*, International Journal of Robotics Research, Sage Publications, vol. 25, no. 10, pp. 985-999, 2006.

[15] C.A. Huang, H.M. Wu and W.H. Hung, *Software/Hardware-based hierarchical finite-time sliding-mode control with input-saturation for an omnidirectional autonomous mobile robot*, IEEE Access, vol. 7, pp. 90254-90267, 2019.

[16] C. Ren, Y. Ding, S. Ma, L.Hu and X. Zhu, *Passivity-based tracking control of an omnidirectional mobile robot using one geometrical parameter*, Control Engineering Practice, Elsevier, vol. 90, pp. 160-168, 2019.

[17] H.M. Wu and M. Karkouh, *Frictional forces and torque compensation-based cascading sliding-mode tracking control for an uncertain omnidirectional mobile robot*, Measurement and Control, Sage Publications, vol. 55, no. 3, pp. 178-188, 2022.

[18] C. Ren, H. Jiang, C. Ma and S. Ma, *Conditional disturbance rejection-based control for an omnidirectional mobile robot: An energy perspective*, IEEE Robotics and Automation Letters, vol. 7, no. 4, pp. 11641-11647, 2022.

[19] C. Ren and S. Ma, *Dynamic modelling and analysis of an omnidirectional mobile robot*, IEEE IROS 2013, Intl. Conf. on Intelligent Robots and Systems, Tokyo, Japan, Nov. 2013.

[20] H. Vellasco-Villa, H. Rodriguez-Castro, J. Estrada-Sanchez, H. Sira-Ramirez and I.A. Vasquez, *Dynamic trajectory tracking control of an omnidirectional mobile robot based on a passive approach*, Advances in Robot Manipulators, InTech Publications, 2010.

[21] K. Watanabe, Y. Shiraishi, S. Tzafestas, J, Tung and T. Fukuda, *Feedback control of an omnidirectional autonomous platform for mobile service robots*, Journal of Intelligent and Robotic Systems, Springer, vol. 22, pp. 315-330, 1998.

[22] M. Diehl, H.G. Bock, M. Diedem and P.B. Wieber, *Fast direct multiple shooting algorithms for optimal robot control*, In: Fast motion in biomechanics and robotics, Lecture Notes in Control and Information Sciences, LNCIS vol. 40, pp. 65-93, 2006.

[23] J.T. Huang, T.V. Hung and M.L. Tseng, *Smooth switching robust adaptive control for omnidirectional mobile robots*, IEEE Transactions on Control Systems Technology, vol. 23, no. 5, pp. 1986-1993, 2015.

[24] A.S. Lafmajani, H. Farivamejad and S. Berman, H_∞ *optimal tracking controller for three-wheeled omnidirectional mobile robots with uncertain dynamics*, IEEE IROS 2020, IEEE Intl. Conf. on Intelligent Robots and Systems, Las Vegas, USA, Oct. 2020.

[25] J. Lafay, C. Collette and P.B. Wieber, *Model predictive control for tilt recovery of an omnidirectional wheeled humanoid robot*, IEEE ICRA 2015, IEEE 2015 Intl Conf. on Robotics and Automation, Seattle, USA, May 2015.

[26] C. Ren and S.Ma, *Generalized proportional integral observer-based control of an omnidirectional mobile robot*, Mechatronics, Elsevier, vol. 26, pp. 36-44, 2015.

[27] M. Sira-Ramirez, C. Lopez-Uriba and M. Velasco-Villa, *Linear observer-based active disturbance rejection control of the omnidirectional mobile robot*, Asian Journal of Control, J. Wiley, vol. 15, no. 1, pp. 51-63, 2013.

[28] S. Lee and D. Chwa, *Dynamic image-based visual servoing on monocular camera mounted omnidirectional mobile robots considering actuators and target motion via fuzzy integral sliding-mode control*, IEEE Transactions on Fuzzy Systems, vol. 29, no. 7, pp. 2063-2076, 2022.

[29] G. Makonnen, S. Kumar and P.M. Pathak, *Wireless hybrid visual servoing of omnidirectional wheeled mobile robots, Robotics and Autonomous Systems*, Elsevier, vol. 75, pp. 450-462, 2020.

[30] G. Rigatos and K. Busawon, *Robotic manipulators and vehicles: Control, estimation and filtering*, Springer, 2018

[31] G. Rigatos and E. Karapanou, Advances in applied nonlinear optimal control, Cambridge Scholars Publishers, 2020

[32] G.G. Rigatos and S.G. Tzafestas, *Extended Kalman Filtering for Fuzzy Modelling and Multi-Sensor Fusion*, Mathematical and Computer Modelling of Dynamical Systems, Taylor & Francis vol. 13, pp. 251-266, 2007.

[33] M. Basseville and I. Nikiforov, *Detection of abrupt changes: Theory and Applications*, *Prentice-Hall*, 1993.

[34] G. Rigatos and Q. Zhang, *Fuzzy model validation using the local statistical approach*, Fuzzy Sets and Systems, Elsevier, vol. 60, no. 7, pp. 882-904,2009.

[35] G. Rigatos, M. Abbaszadeh and M.A. Hamida, *Intelligent control for electric power systems and electric vehicles*, Taylor and Francis / CRC Publications, 2024.

[36] G. Rigatos, *Nonlinear control and filtering using differential flatnesss theory approaches: Applications to electromechanical systems*, Springer, 2016

[37] G.J. Toussaint, T. Basar and F. Bullo, H_∞ *optimal tracking control techniques for nonlinear underactuated systems*, in Proc. IEEE CDC 2000, 39th IEEE Conference on Decision and Control, Sydney Australia, 2000.

[38] G. Rigatos, M. Abbaszadeh, P. Siano, *Control and estimation of dynamical nonlinear and partial differential equation systems*: Theory and Applications, IET Publications, 2022

[39] G. Rigatos, M. Abbaszadeh and J. Pomares, *Flatness-based control in successive loops for electropneumatic actuators and robots*, IFAC Journal of Systems and Control, Elsevier, vol. 25, pp. 10222, 2023.

[40] G. Rigatos, P. Wira, M. Abbaszadeh and J. Pomares, *Flatness-based control in successive loops for industrial and mobile robots*, IEEE IECON 2022, IEEE 2022 Intl. Conf. on Industrial Electronics, Brussels, Belgium, Oct. 2022.